UNIVERSIDADE DE LISBOA

FACULDADE DE CIÊNCIAS

DEPARTAMENTO DE ENGENHARIA GEOGRÁFICA, GEOFÍSICA E ENERGIA

Shear wave velocities in a construction landfill

Mestrado em Ciências Geofísicas

Especialização em Geofísica Interna

Joana Filipa Formigo Santos

Dissertação orientada por:

Prof. Doutor. Luís Manuel Henriques Marques Matias

Dr. Hélder Jorge Tareco Hermosilha

2016

Acknowledgements

I would like to thank Dr. Luís Matias and Hélder Hermosilha for having accepted to be my advisers during this final stage of my Master's degree. Dr. Paula Costa and Dr. Fernando Marques who helped me with the bibliographic research. A very special thank you to all my work colleagues at Geosurveys, who helped me in this period with their knowledge and companionship. Jaime Machado, who helped me and motivated me during this troubled year. And finally, to my family, who supported my decisions and enabled me to finalize my thesis.

Abstract (resumo em Inglês)

This report presents the Multichannel Analysis of Surface Waves (MASW) on a construction landfill. The main goal of the survey is to determine the shear wave velocities (V_S) in order to estimate the dynamic properties of the soil. The velocity of shear waves (V_S) were obtained from the Rayleigh wave's dispersion. The present document reports the acquisition and processing of 28 seismic profiles (approximately 3225 m for MASW data) acquired between March and July 2015. In the acquisition, a linear array of 24 geophones spaced by 1.2 m was used for the active measurements. Since the method uses vertical impulse (PEG 40 and sledge hammer) and vertical recording, it was also possible to determine the compressional wave velocities derived from refraction analysis, using the *Rayfract Seismic Refraction & Borehole Tomography® software.* The 2D compressional wave models were used to infer the thickness/ geometry of the layers, as well as preliminary input for MASW data processing /modeling, since applying an *a priori* model minimizes the dispersion of the final results. The processing consists of two main stages: imaging dispersion curves of surface waves and the estimation of near-surface shear-wave velocity by inversion of Rayleigh waves. Finally, a 2D S-wave velocity section was generated due to the CMP roll-along acquisition format. For the gridding process, the Golden Software's Surfer® was used, placing each S-wave profile (V_S versus depth) in the middle of the seismic spread with which it was calculated. Finally, each line was placed in its location and represented *Voxler 3 3D software®*, allowing a better perception of the distribution of the dynamic properties of the soil along the landfill. Shear wave velocities (V_S) generally increase with depth, but they can differ due to site conditions, water content, tide levels, landfill operation procedures, like compaction made on site, among others.

Key-words: MASW, Surface Waves, Shear waves, Landfill

Resumo (resumo em Português)

Com este trabalho pretende-se determinar a velocidade das ondas de cisalhamento (V_S) num aterro através do método da análise multicanal de ondas de superfície (MASW), estimando consequentemente as propriedades dinâmicas do solo. A velocidade das ondas de cisalhamento (V_S) foram obtidas a partir da dispersão das ondas de Rayleigh.

O presente documento relata a aquisição e processamento de 28 perfis sísmicos adquiridos entre Março e Julho de 2015. Na aquisição foi usado um conjunto de 24 geofones verticais com uma frequência natural de 10 Hz. Os recetores estavam ligados entre si com um espaçamento de 1,2 m, sendo deslocados em conjunto 4.8 m após a realização de um par de tiros. Por cada posição foram realizados 2 tiros, com diferentes distâncias ao primeiro geofone, 2.4 e 9.6 m, mas apenas o tiro mais afastado (9.6 m) foi usado para a obtenção das ondas S com o método MASW. De acordo com as condições do sítio, a fonte utilizada foi a PEG-40 ou um martelo.

Uma vez que o método utiliza um impulso vertical e receção vertical, também foi possível determinar a velocidade das ondas longitudinais (V_P), derivadas da análise de refração usando o *software Rayfract Seismic Refraction* & *Borehole Tomography* ®. Para este método, ambos os tiros com diferentes distâncias foram usados para a análise das ondas refratadas. Os modelos de ondas de compressão 2D foram utilizados para aferir a espessura e número de camadas, como modelo preliminar para o processamento em MASW. A inserção de um modelo *a priori* permite uma melhor modelação da curva

de dispersão ao espectro de velocidades, minimizando assim a dispersão dos resultados após a inversão.

Para a inserção dos dados no *software Rayfract Seismic Refraction* & *Borehole Tomography*, todas as distâncias e posicionamentos inerentes à aquisição tiveram de ser convertidos em números de estações, utilizando como unidade de medida a distância entre geofones. Estabeleceu-se como estação 0 a posição do geofone mais próximo do tiro (G1).

Para a obtenção dos modelos 2D da velocidade das ondas compressivas, foram picadas as primeiras chegadas.

Posteriormente, criou-se um modelo de camadas baseado no modelo de ondas refratadas para a análise das ondas superficiais. O processamento das ondas superficiais consiste basicamente em duas etapas principais: (1) obtenção do espectro de velocidades, que corresponde à dispersão da energia relacionando a frequência com a velocidade de fase. Neste espectro de velocidades podem-se distinguir diversos modos de propagação das ondas superficiais, no entanto só o modo fundamental foi picado; Posteriormente segue-se (2) a estimativa da velocidade de cisalhamento através da inversão do modelo *a priori* criado. Finalmente, os perfis 2D da velocidade das ondas s foram gerados devido à aquisição em série realizada. Para o processo de interpolação espacial, utilizou-se o Golden Software Surfer®, onde cada perfil vertical V_S foi representado no meio dos 24 geofones, entre o 12º e o 13º.

Com o método MASW produziram-se cerca de 695 perfis verticais 1D para as ondas S, perfazendo um comprimento total de 3225 m. Na refração, para o cálculo da velocidade das ondas P, foram utilizados 1396 tiros, resultando num comprimento total de 4267 m.

Finalmente, cada modelo 2D de velocidade das ondas S foi representada por um *software* 3D - *Voxler 3*, permitindo assim uma melhor perceção da das propriedades dinâmicas do solo ao longo do aterro.

Através da disposição dos modelos verifica-se que o substrato rochoso vai ficando mais profundo à medida que se aproxima do mar, sendo também visível que a espessura de sedimentos do aterro é maior junto à costa do que para o seu interior. Fazendo um balanço geral, as linhas adquiridas em épocas diferentes apresentam velocidades diferentes nos sedimentos do aterro, nomeadamente os perfis adquiridos em Março apresentam velocidades cisalhantes inferiores aos adquiridos em Junho e Julho. Este facto pode dever-se à água presente no solo derivada da época das chuvas, que ocorre em Março. Ademais, os perfis mais próximos da costa apresentam velocidades inferiores a todos os outros perfis, independentemente da data de aquisição, e da energia de compactação inerente ao local. A velocidade das ondas de cisalhamento (V_S) tende a aumentar com a profundidade, mas pode diferir com as condições do local, mais precisamente com a presença de água decorrente das chuvas ou da variação do nível de marés. As heterogeneidades na compactação de aterros também podem influenciar a sua velocidade.

Neste trabalho, as inversões de velocidades podem ser vistas em todos os modelos 2D da velocidade das ondas S, entre os 0 m (MSL) até à base rochosa. Esta inversão encontra-se na mesma cota do nível freático e reflete, provavelmente, as variações das marés. Esta camada de baixa velocidade acima do substrato rochoso, em ocasiões de chuvas intensas, pode tornar ainda mais baixa a resistência ao cisalhamento.

Para uma análise mais aprofundada da velocidade das ondas S, foram escolhidos três perfis: L01, L02 e L06 de modo a compará-los entre si. No L02, fez-se um levantamento das marés referentes aos 2 dias de aquisição, com o objetivo de analisar o efeito das marés na velocidade das ondas s. Nesta análise foi visível a mudança de maré que existia entre os dois dias de aquisição. Posteriormente, realizou-se uma comparação entre os perfis L01 e L02 de modo a perceber a influência da época das

chuvas no comportamento do aterro. Feita a comparação, foi possível verificar que L01, adquirida em Março, atingia uma velocidade mínima na inversão de 245 m/s, enquanto L02, adquirida em Junho, atingia uma velocidade mínima de 293 m/s, mesmo estando o perfil L02 situado numa zona de maior energia de compactação.

Por fim compararam-se dois perfis adquiridos na mesma época, mas que se localizavam em zonas com diferentes energias de compactação: L01 e L06. As velocidades mínimas atingidas na camada de inversão não diferem significativamente, sendo em L06, V_{Smin}=217 m/s. No entanto, apesar da energia de compactação do local onde L06 foi adquirida ser muito superior à do local onde a linha 01 foi adquirida, as velocidades cisalhantes do aterro não se apresentam superiores no modelo 2D obtido. Possivelmente a proximidade à costa e consequente influência da água, tenha maior impacto na variação da velocidade do que a energia de compactação. No entanto é possível verificar no perfil L06, uma mudança de velocidade entre as zonas com diferentes energias de compactação.

Relativamente a análise do V_{S30}, todos os modelos apresentam valores superiores a 360 m/s, o que classifica o solo como muito denso ou como rocha "macia", no entanto os perfis são muito heterogéneo sentre si..

Para uma melhor avaliação dos dados e classificação do terreno, seria vantajoso realizar uma série de análises ao aterro depois de compactado, como perfuração, ensaios *in situ*, SPT, amostragem e os ensaios de laboratório. Estas análises possibilitariam uma comparação da velocidade das ondas S com modelos empíricos utilizando os ensaios SPT. Inclusive, o cálculo do modo de distorção seria mais verossímil caso fossem disponibilizados valores da densidade.

Palavras-chave: MASW, Ondas superficiais, Ondas S, Aterros

Table of Contents

List of Figures

List of Tables

Abreviations

1D – 1-Dimensional
2D – 2-Dimensional
3D – 3-Dimensional
AWD – Accelerated Weight Drop
Acq - Acquisition
DGPS – Differential Global Positioning System
GA – Genetic Alhorithms
GI – Geophone Interval
ID – Identification
MASW – Multichannel Analysis of Surface Waves
MPPD - Marginal Posterior Probability Density
MSL – Mean Sea Level
PEG – Propelled Energy Generator
QC – Quality Control
RMS- Root mean square
SEG-2 – Convention from the Society of Exploration Geophysicist (SEG) for raw or processed shallow seismic or digital radar data
SNR – Signal to Noise Ratio
S/R – Source/Receiver
UTM – Universal Transverse Mercator
WET – Wavepath Eikonal Traveltime inversion

1. Introduction

During my internship in the company: Geosurveys Portugal – Geophysical Consultants, I had the chance to do my thesis with the data obtained on a MASW Survey realized on a company project. Regarding that fact, the location and identification of the survey area are confidential. During this work, I establish a method to get reliable results from the multichannel analysis of surface waves, which include a previous refraction analysis.

1.1. Soil characterizations

The geomechanical characterization of the shallow layers is very importante to understand the location in study. The near surface P and S-wave seismic velocities provide valuable information for studies of ground motion behavior. [Carvalho et al., 2009; Akin et al., 2011] Where the shear wave velocity is a fundamental parameter required to define the dynamic properties of soils. It is useful in the evaluation of foundation stiffness, earthquake site response, liquefaction potential, soil density, site classification, soil stratigraphy and foundation settlements. [Akin et al., 2011] There are several methods for estimating shear waves, such as borehole logging, seismic reflection profiles or surface wave's inversion. [Carvalho et al., 2009] However, shear wave velocities of soil profiles are most accurately determined using in-situ seismic measurements because in-situ measurements involve very low strain levels, and the measured values can be used to obtain the maximum shear modulus (G_{max}) at a particular depth in a soil deposit. The small strain shear modulus, G_{max} is an important parameter in seismic analyses of landfills and is also related to the compressibility of municipal solid waste. It can be calculated using elasticity theory through the following equation: [Akin et al., 2011; Hanumantharao, C., & Ramana, G. V., 2008]

$$G_{max} = \rho {V_S}^2$$

In the absence of a soil's density value it can be assumed, since slight variation of density has a small influence in the estimated value. [Hanumantharao, C., & Ramana, G. V., 2008]

1.2. Refraction surveying

The P-wave refraction survey was conducted mainly for the geometrical characterization of the structures of the landfill. The very shallow water table limits the P-wave velocity variations in the saturated soft sediments, and the primary objective of the test was the identification of the base of the soft sediments. The acquisition geometry was designed considering the desired investigation

depth. Long spreads for P-wave refraction were used to achieve greater investigation depth and identify possible lithological boundaries below the water table and lateral variation.

1.3. Refraction method

The seismic refraction is a fast, efficient and non-invasive method. This method is based on the generation of seismic P waves that propagates on the subsoil and refract in the interfaces with increasing propagation velocities in depth, and with sufficiently different elastic characteristics. The major limitation of this method is that it cannot identify a low speed layer in the middle of two layers with higher speeds. Which means that the velocity of propagation of P-waves has always to increase in depth. [Redpath, 1973].

1.4. *MASW surveying*

The software winMASW® allows analyzing seismic data to determine the vertical profile of the shear waves. The MASW method is based on the phenomenon of dispersion study of surface waves. [Neves et al., 2014]

1.5. Surface Waves

The surface waves result from the interaction between P and S waves when they reach a surface. These propagate along the surface, decreasing its amplitudes almost exponentially when they go deeper. The surface wave are dispersive, i.e. different frequencies propagate with different speeds, known as phase velocity. (Neves et al., 2014)

Mainly, there are two types of surface waves: Rayleigh and Love waves. In this thesis only the Rayleigh waves will be discussed. Surface wave methods are especially appealing in measuring V_S in landfills, because they are non-intrusive method. The shear wave velocities can be derived from inverting the dispersive phase velocity of surface waves using a process called multichannel analysis of surface waves (MASW). (Xia et al., 2004)

1.5.1. MASW Processing

MASW estimates S-wave velocity from multichannel vertical component data. It consists in three parts: 1) data acquisition; 2) dispersion-curve picking and 3) Inversion. Furthermore, a 2D S-wave velocity section can be generated when surface wave data are acquired in a standard CMP roll along acquisition format.

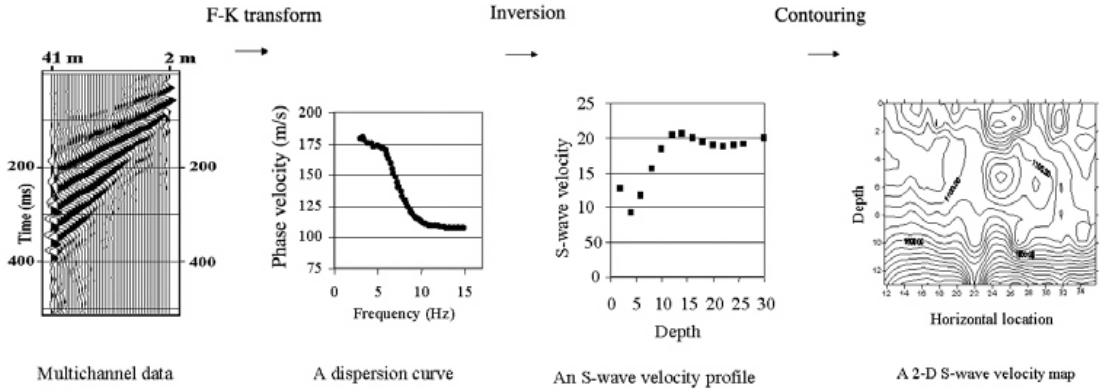

Figure 1- MASW Processing sequence. [Xia et al., 2014]

- **Surface-wave data acquisition**

The type of surface waves acquired depends on the source, direction of impact and geophones orientation. When the source is a vertical impact and geophones are vertical component, the surface waves analyzed are Rayleigh. The maximum penetration depth in a homogeneous medium is about one wavelength [Elisoft – geophysical software and services, 2015]. The currently accepted rule of thumb for the maximum penetration depth is approximately half the longest wavelength. Normally, the longer the geophone spread, the higher the resolution of the dispersion image. To avoid spatial aliasing, the receiver spacing should be less than half the shortest measured wavelength.

- **Dispersion curves of surface waves on multi-channel record.**

In this step, proceeds to the picking of the dispersion curve in the F-V domain or F-K domain. The conversion is made through the relation: $v = \frac{f}{k}$, where v is the phase velocity associated to the frequency f and wave number k. [Dal Moro et al., 2003] $F - K$ spectrum consists in an image representing the energy density. This image uses the colour intensity to show the amplitudes of the data at different frequency and wave-number components. Moreover, as the wave field is only characterized by Rayleigh waves, it is possible to see several propagation modes, reliable separated; which is possible only through a multi-channel recording method combined with an appropriate multi-channel data-processing technique [Tselentis & Delis , 1998]. Such curves are later used for the inversion process, which eventually provides subsurface information of use in geological or geotechnical applications [Dal Moro et al., 2003]

- **Inversion of dispersion curves of surface waves**

The Rayleigh-wave phase velocity of a layered earth model is a function of frequency and four earth properties: P-wave velocity (V_P), S-wave velocity (V_S), density (ρ), and thickness of layers (h).

$$F(f, c, V_S, V_P, \rho, h) = 0$$

Where f is the frequency in Hz, c is the Rayleigh wave phase velocity at frequency f.

Analysis of the Jacobian matrix provides a measure of dispersion-curve sensitivity to these earth properties where shear-wave velocity is the dominant influence on a dispersion curve in the high-frequency range (>2 Hz), therefore only S-wave velocities are considered unknowns in the inversion. [Xia et al., 1999]

The disadvantage of the inversion method is the non-uniqueness of the solutions, namely the possibility of obtaining many layers, relatively close to the solution, which satisfy the observed data. For this method to be applied successfully, it is necessary to restrict some parameters, like establishing an initial starting model for the inversion process, to minimize the dispersion of the final result. This initial model might be defined using the layer thicknesses obtained by other seismic the methods, like refraction for example. [Neves et al., 2014]

However, in the processing software used, the method used for the inversion of the dispersive curve is based on an optimization process (genetic algorithms) [Dal Moro, 2007).] This method implemented a two-step inversion, the first one starts with several preliminary "parallel" runs and the second one uses the previously determined fittest model as starting population. (Figure 2)

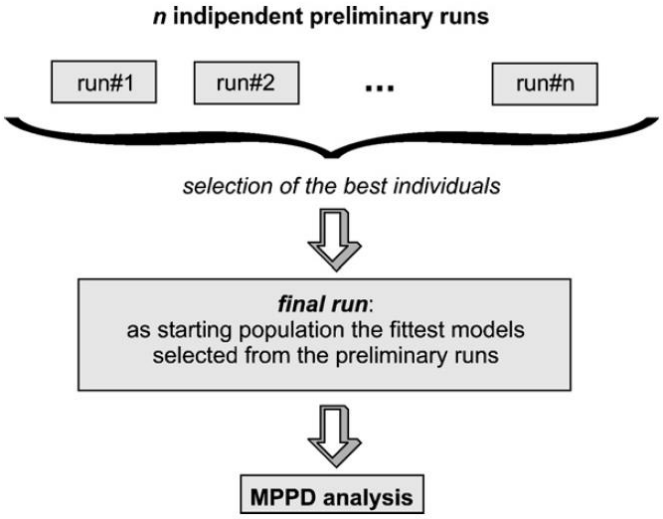

Figure 2- Genetic Algorithms sequence for surface wave analysis

The key element for any kind of optimization is the model evaluation, which is performed by means of an objective function that allows a quantitive estimation of the model. For that it's considered the RMS value of the difference between the observed and calculated phase velocities, i.e. the dispersion curve.

$$Objective\ Function = -\sqrt{\frac{\sum_{i=1}^{n}\left(v_{obs,i} - v_{cal,i}\right)^2}{n}}$$

where n represents the number of observed frequency– velocity couples, $v_{obs,i}$ the observed phase velocity at the ith frequency and $v_{cal,i}$ the calculated velocity for the considered model (individual of the current population).

- **2D S-wave velocity sections.**

If surface wave data are collected in a CMP roll-along acquisition fashion, a 2D S wave velocity section can be generated with gridding software by placing each S-wave profile (V_S versus depth) in the middle of the geophone spread with which it was calculated. [Xia et al., 2004]

1.6. S- waves

$V_{S,30}$ can be estimated using existing V_S measurements. The results in terms of $V_{S,Z}$ i.e. time-average shear wave velocity in the topmost z meters are calculated according to:

$$V_{S,Z} = \frac{Z}{\sum_{i=1}^{N} \frac{H_i}{V_{S,i}}}$$

in which N is the number of layers used for the discretization of the model from the surface to z and H_i and $V_{S,i}$ are the thickness and shear wave velocity for each layer i, respectively. Moreover $V_{S,Z}$ can be used to compare the expected site amplification for two different shear wave velocity profiles.
The Next Generation Attenuation ground motion prediction equations use the shear wave velocity of the top 30 m of the subsurface profile ($V_{S,30}$) as the primary parameter for characterizing the effects of sediment stiffness on ground motions.
The Caltrans Seismic Design Criteria classifies sites based on VS of the top 30 m of the soil profile (V_{S30}). Sites are divided into the six categories (Soil Profile Types A through F) presented in Table 1.
[Wair, B. R. & DeJong J. T., 2012]

Table 1- Soil Profile Types

Site Class	Soil Profile Name	V_{S30}
A	Hard Rock	>1500 m/s
B	Rock	760 to 1500 m/s
C	Very dense rock and Soft Rock	360 to 760 m/s
D	Stiff Soil	180 to 360 m/s
E	Soft soil	<180 m/s
F	Soils Requiring Site Specific Evaluation	-

Statistical correlations between V_{S30} and surficial geology can be done for site characterization.

1.7. Purpose and objectives of the survey

This survey was performed in a construction landfill, aiming to evaluate the dynamic response of the soil, through the estimation of the shear wave velocities. The velocities of the shear waves were obtained from the Rayleigh wave's dispersion using the Multichannel Analysis of Surface Waves method (MASW). Additionally, and because the method uses vertical impulse and vertical recording, it was also possible to determine the compressional wave velocity (from refraction analysis).

2. SITE CONDITIONS

As said before, the location and identification of the survey area in this study is confidential, so the geological context, as well as its representation, will be without coordinates or other identifying information.

2.1. Topography and Geomorphology

The survey area is near the coastline represented in Figure 3. Onshore site develops according to the continental tectonics, where erosion landforms are structural plains, which were built due to the slow increase of the sedimentary thickness of the crust and the continuous rise of the water level.
The site is mainly on the highlands of flat top surface with an absolute elevation of over 200 m, known as a plateau, which belongs to one type of structural plain. The site gradually becomes hilly terrain from east to west and develops into coastal cliffs when meeting the coastline. Some parts of the site are explored areas of limestone which develop karst topography such as cavities, sink holes and slump zones. Concerning the mass movements, a large number of seasonal streams flow from east to west, where the drainage patterns across the site are typically dendritic and are characterized by irregular branching of tributary control.
The coastline is made up of long sandy beaches interrupted by rocky shores and steep cliffs that rise about 120 meters above sea level. The offshore site develops coastal erosion landform, whose type is called wave cut terrace – this inclines towards the sea and its outer edge and is roughly parallel to the coastline.

Figure 3- *Location of the area before the construction of the landfill. (Image adapted from Google Earth)*

2.2. Regional Geology

The regional geology is dominated by Proterozoic formation, whilst Neoproterozoic formation occurs in the western part of the country. The onshore section is characterized by a transformed margin which has a distinctive, mainly progradational stratigraphic architecture with long-term sedimentary gaps and high-elevation marine terraces resulting from moderate Upper Cretaceous–Cenozoic to major Quaternary uplifting. Margin style also governs spatial variations in the volume of offshore sediment dispersed in the associated deep-sea fans.
The age and lithology of the geological formations existing in the survey area are the following:

- Holocene marine deposits: sand, gravel, clay, etc.
- Cenomanian-turonian: oolitics and pisolitic limestones, marl (mudstone) and conglomerate.
- Cenomanian: limestone, oolites, dolomite and conglomerate.
- Albian: limestones, marl (mudstone) and gypsum conglomerates.
- Apcian: marl (mudstone), limestone and gypsum.

2.3. Field Tests and landfill construction

A geotechnical survey was conducted in the area before the construction of the landfill, including drilling, *in situ* tests, SPT, sampling and laboratory tests.
That investigation classified the site stratigraphic according to the following:
Soil layers:

a. Marine deposits;
b. Loose, fine-grained, silty sand;
c. Very soft clay.

Rock units:

d. Moderately weathered Limestone;
e. Moderately weathered Mudstone;

Before the construction of the landfill, the harbor basin was dredged. After the excavation, there were mainly two sorts of rock units: moderately weathered limestone (d) and moderately weathered mudstone (e).
All the soil layers were removed completely before the construction of the quay (Figure 4).

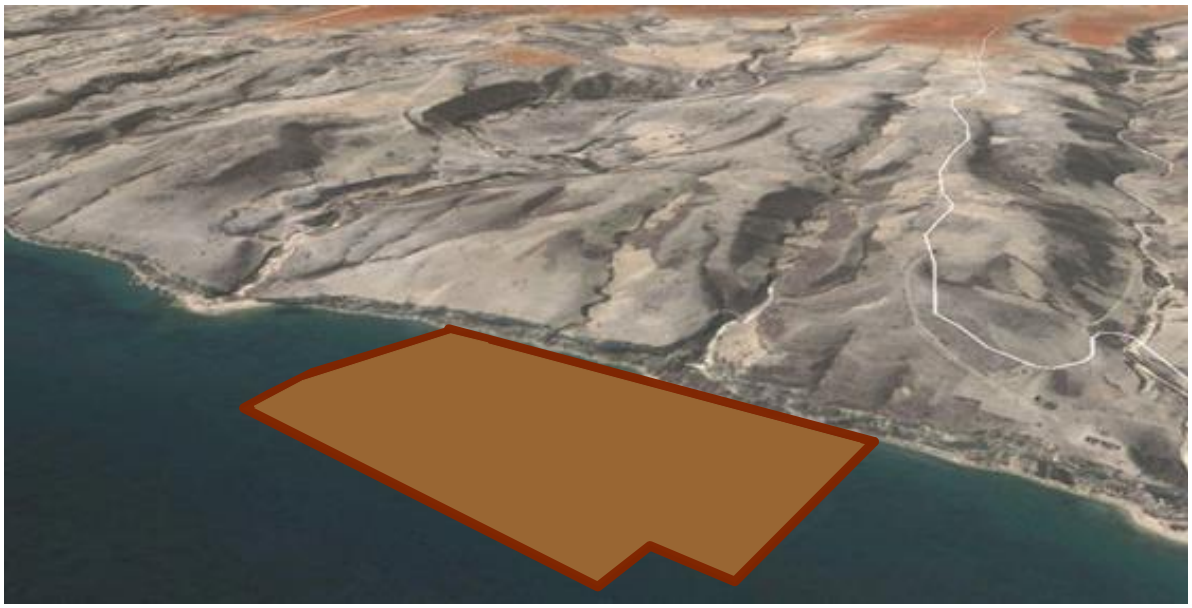

Figure 4*- Location of the area after the construction of the landfill. (Image adapted from Google Earth)*

2.4. Compaction of the landfill

During the construction, the landfill was compacted. The aim of the compression of the landfill is to increase the resistance to the strain disturbance of the soil under the action of external forces; reduce possible volumetric variations, reducing the empty spaces and consequently the water absorption capacity and the percolation decreases, making the soil more stable.
There is no information regarding the moisture content, but concerning the area compression, Figure 5 shows a representative scheme of the compression energy inherent to the survey area. [Das, B. M., (2010)].

Figure 5- Disposition of the different compaction energies along the survey area.

The primary technique used in the compaction of the landfill was the dynamic compaction. This process consists primarily of dropping a heavy weight repeatedly on the ground at regular intervals. The weight of the hammer used varies over a range of 80 to 360 kN, and the height of the hammer drop varies between 7.5 and 30.5 m. The stress waves generated by the hammer drops aid in the densification. The degree of compaction achieved at a given site depends on the following three factors: 1). Weight of hammer; 2). Height of hammer drop and on the 3). Spacing of locations at which the hammer is dropped. However there are no references regarding this values. [Das, B. M., (2010)].

3. DATA ACQUISITION

The present document reports the acquisition and processing of 28 seismic profiles, acquired between March and July 2015, using geometries favorable to the refraction and MASW methods.
The survey was conducted along the profiles shown in Figure 6 and, despite the acquisition orientation, the seismic lines are mostly oriented NNE-SSW with a maximum length of 354 m.

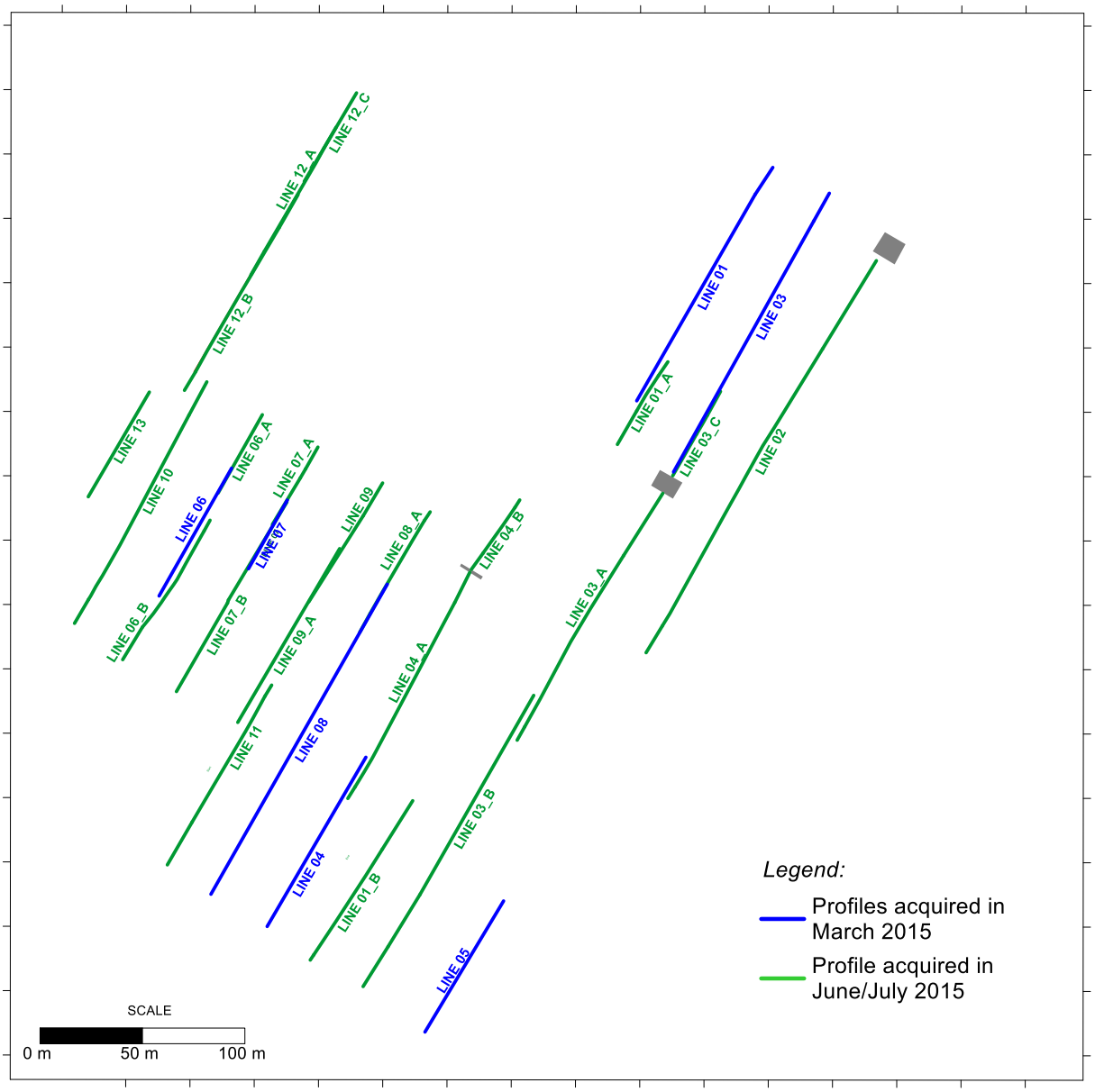

Figure 6 – Survey seismic profiles acquired in March 2015 (blue lines) and June/July 2015 (green lines) (WGS84).

3.1. Equipment and Data Acquisition Parameters

The equipment and data acquisition parameters were carefully selected in order to meet the requirements and goals of the project. The energy was generated by two different sources used during the survey: the Accelerated Weight Drop (AWD) seismic source PEG-40 and the sledgehammer + base plate. The source used for each shot was selected according to the weather and site conditions/limitations. The land streamer used had 24 channels (vertical geophones) spaced 1.2 m, with a total active length of 27.6 m, and the recorder was an exploration seismograph Geode 24 channels (Figure 7). The acquisition parameters are summarized in Table 2.

Table 2– Equipment and data acquisition parameters.

Source 1	***AWD PEG 40***
Weight	*40 kg*
Number of stacked Shots per offset	*1-2*
Source 2	***Sledgehammer***
Weight	*5 kg*
Number of stacked Shots per offset	*5*
Shot Offset	*2.4, 9.6 m*
Streamer	***Land Streamer***
Number of channels	*24*
Geophone Interval (GI)	*1.2 m*
Total Active Length	*27.6 m*
Geophone	*OYO 10 Hz*
Geophone Type	*Vertical*
Recorder	***Geode 24*** *from Geometrics*
Sampling Rate	*0.125ms*
Record Length	*1.5 s*
Format	*SEG-2*
GPS	***Trimble R8 DGPS*** *receiver with base station*

(a) (b)

Figure 7 – *Equipment used in data acquisition. a) Geod 24 from Geometrics b) Accelerated Weight Drop PEG-40*

3.2. Geometry

To process the refraction data, *Rayfract®* software was used. This has the particularity of using station numbers, instead of real distances, to define the shots and geophones' positions. Regarding that fact, the geophones' spacing of 1.2 m was used as the measuring unit of all the remaining positions/distances. To accomplish this limitation, a multiple offset geometry was used, along with the source and the first geophone distanced by 2.4 m and 9.6 m, respectively offset 1 and offset 2 (Figure 8). The multiple offsets, at 2.4 m and 9.6 m, had the aim of increasing the resolution on shallow layers and of achieving greater depths of investigation, respectively.
For the refraction P wave, two shot offset were processed, however, for the MASW, only the larger shot offset was used to guarantee the desired investigation depth.
In order to increase the signal to noise ratio, for each offset 2 or 5 shots were stacked, according to the selected source (2 stacks using PEG-40 and 5 with the sledgehammer).

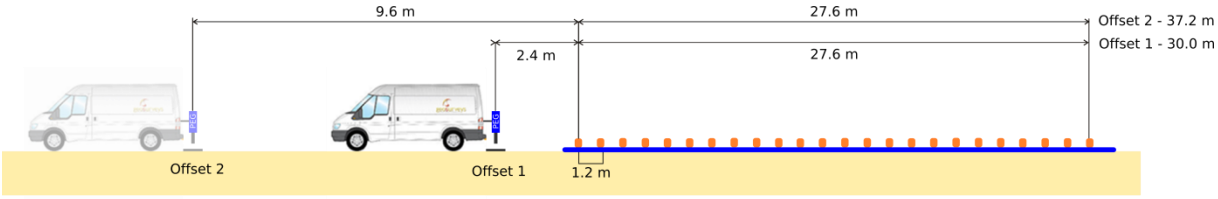

Figure 8 – Offset diagram of the seismic spread used for the survey (not to scale).

The space increment along the line was set at 4.8m (spread advance in line); meaning, when the two shots for that spread position are executed, the system is moved forward 4.8m and a new set of shots, in the 2 different offsets, are executed (Figure 9).

The raw recorded data has the geometry assigned for each shot in distance. These distances were converted into stations with intervals of 1.2 m (minimum station spacing). Figure 9 shows the relation between source and receiver positions and their respective distances and station numbers.

Station number	23	22	21	20	19	18	17	16	15	14	13	12	11	10	9	8	7	6	5	4	3	2	1	0	-1	-2	-3	-4	-5	-6	-7	-8	-9	-10	-11	-12	-13	-14	-15	-16	-17	-18	-19	-20
Distance (m)	-27.6	-26.4	-25.2	-24.0	-22.8	-21.6	-20.4	-19.2	-18.0	-16.8	-15.6	-14.4	-13.2	-12.0	-10.8	-9.6	-8.4	-7.2	-6.0	-4.8	-3.6	-2.4	-1.2	0.0	1.2	2.4	3.6	4.8	6.0	7.2	8.4	9.6	10.8	12.0	13.2	14.4	15.6	16.8	18.0	19.2	20.4	21.6	22.8	24.0
Shotposition 1	G24	G23	G22	G21	G20	G19	G18	G17	G16	G15	G14	G13	G12	G11	G10	G9	G8	G7	G6	G5	G4	G3	G2	G1		S1						S2													
Shotposition 2					G24	G23	G22	G21	G20	G19	G18	G17	G16	G15	G14	G13	G12	G11	G10	G9	G8	G7	G6	G5	G4	G3	G2	G1		S3						S4									
Shotposition 3									G24	G23	G22	G21	G20	G19	G18	G17	G16	G15	G14	G13	G12	G11	G10	G9	G8	G7	G6	G5	G4	G3	G2	G1		S5						S6				
Shotposition 4													G24	G23	G22	G21	G20	G19	G18	G17	G16	G15	G14	G13	G12	G11	G10	G9	G8	G7	G6	G5	G4	G3	G2	G1		S7						S8

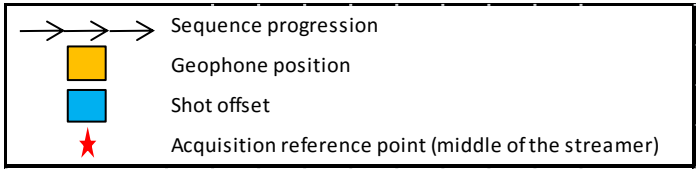

Figure 9– Source (blue) and receiver (orange) geometry for 4 shot positions showing the distance between shots, geophones and the stations used for processing.

3.3. Line Identification

The lines were identified by the line number (e.g. L01) followed, if applicable, by the portion of the line "_A" or "_B" stem (e.g. L01_A). The following table (Table 3) shows the line ID used henceforth in this report, the month of acquisition, the number of shots, the line length in meters for both methodology refraction and MASW. Some of the lines acquired in different days were merged whenever they match the following criteria:

- Correspondence to a continuation of a previous line (have the same alignment, without a lateral shift);
- Have the same topography (the topography did not change due to an addition of construction landfill material);
- The lines are acquired within a short period of time in order to have a similar level of compaction and water content.

Table 3 - Line identification from acquisition and processing ID.

Line ID	Acquisition Month	Number of shots	Total shots	Refrac. Line Length (m)	MASW Line Length (m)
L01	Mar	73	73	210	172.8
L01_A	Jun	18	18	75.6	38.4
L01_B	Jun	26	48	147.6	110.4
	Jun	22			
L02	Jun	60	135	354	316.8
	Jun	75			
L03	Mar	91	91	248.4	211.2
L03_C	Jun	63	18	75.6	38.4
L03_A			80	224.4	187.2
	Jun	68			
L03_B	Jun	62	98	267.6	230.4
	Jun	36			
L04	Mar	50	50	152.4	115.2
L04_A	Jun	70	70	200.4	163.2
L04_B	Jul	14	14	66	28.8
L05	Mar	36	36	118.8	81.6
L06	Mar	34	34	114	76.8
L06_A	Jul	16	16	70.8	33.6
L06_B	Jul	40	40	128.4	91.2
L07	Mar	12	12	61.2	24
L07_A	Jul	16	16	70.8	33.6
L07_B	Jul	58	58	171.6	134.4
L08	Mar	102	102	277.2	240
L08_A	Jun	32	32	109.2	72
L09	Jun	32	32	109.2	72

L09_A	Jul	52	52	157.2	120
L10	Jun	70	70	214.8	177.6
L11	Jul	54	54	162	124.8
L12_A	Jul	42	42	133.2	96
L12_B	Jul	60	60	176.4	139.2
L12_C	Jul	18	18	75.6	38.4
L13	Jul	26	26	94.8	57.6

3.4. Navigation and Positioning

A criterious positioning procedure was made. The topographic survey was carried out using a RTK system. A measurement (x y, and z) was performed at the 1st shot position and for geophones 1, 12 and 24 (G01; G12; G24; S01 in Figure 9); at the last shot position and again for geophones 1, 12 and 24 (G01'; G12'; G24'; S##'); and in areas with curves in the profile and topographic variations, such as trenches or slopes (Figure 10). The positioning was based on the WGS84 datum and the elevations are relative to Mean Sea Level (MSL).

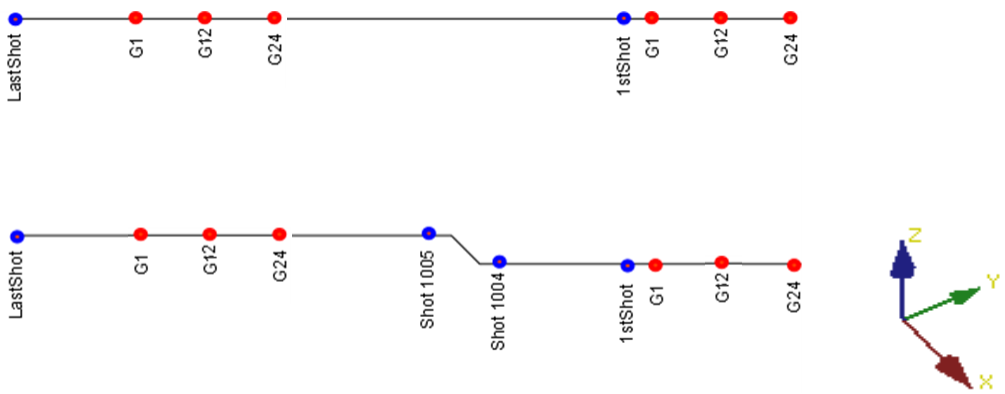

Figure 10- Representation of the measurement positions acquired according to the topographic variations. The blue points represent shot positions and the red ones geophone positions in the landstreamer.

Although the survey area is relatively flat and all the lines range from 2 to 4 m above sea level, the same profile of the topographic variations is always less than 1 m.

3.5. Data Acquisition Constraints

During daytime there was construction work in progress on the site. Therefore, the MASW survey was conducted at night in order to avoid ambient/seismic noise. The acquisition was sometimes constrained by obstacles in the planned lines, adverse weather conditions and infrastructures, such as trenches (Figure 11). Small curves or even small spatial shifts from the planned profile were made when it was necessary to bypass some obstacles (vehicles or pavement bricks - Figure 12).

For example, in the case of a trench, besides the position of the geophones G01, G12 and G24, other geophone positions had to be measured in order to get all the topographic variations.

(a) (b)

Figure 11 – *Example of topographic constraints: (a) trench and (b) topographic slope.*

(a) (b)

Figure 12 – *Example of obstacles that forced a spatial shift in the profile: (a) presence of a vehicle and (b) pavement bricks.*

4. SIGNAL ANALYSIS

In order to ensure that the data could be processed successfully, all the acquired seismic data underwent a thorough quality control procedure of the signal quality, positioning and acquisition geometry. The following QC was implemented for each line:

- Refracted wave check for selected shots by a shot to gather analysis;
- Noise analysis and signal saturation assessment;
- Positioning quality control – the lines have to follow some requirements, such as overlapping with previous acquired profiles, matching what was planned or, if the profiles do not match due to constraints/obstacles in the field, they should have been approved;
- The geometry needs to be respected and checked before processing. Therefore, the source and receiver offset was controlled for each land shot, in order to ensure that the chosen geometry was preserved.

4.1. Source Analysis

Due to the weather conditions, the landfill was muddy, which made it difficult to use of the van and, consequently, the PEG-40. As a result, some shots had to be done with another source – the sledgehammer. In the L03, eight shots (10169-10176) were acquired with a sledgehammer. Hence, in order to understand which frequency is generated from the two sources, the frequency spectrum of the sources is described below (Figure 13).

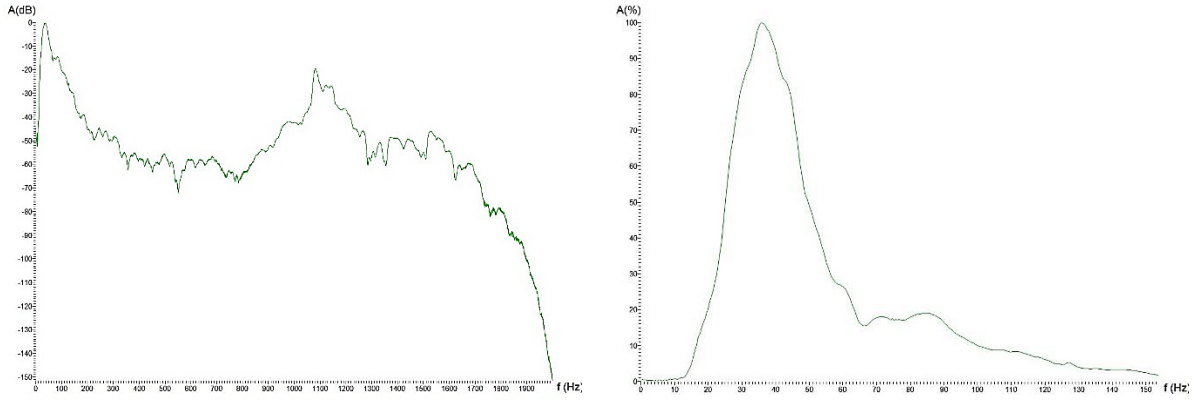

(a)

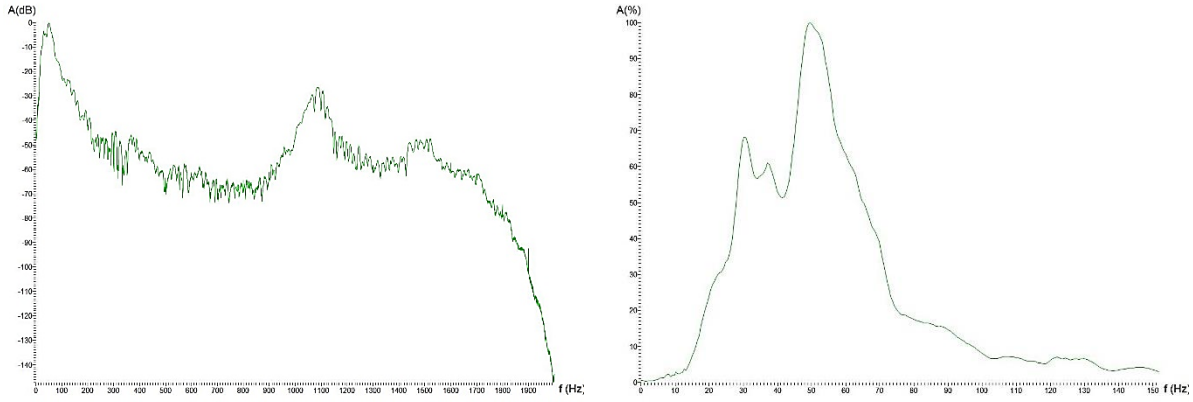

(b)

Figure 13 – a) Frequency spectrum of Source 2-Sledgehammer regarding the 10070 of L03 and b) Frequency spectrum of Source 1-PEG 40 regarding shot 10018 of L03.

The amplitude spectrum analysis allows the identification of the dominant frequency or period corresponding to the maximum amplitude value. Considering the two spectrums, it is possible to conclude that PEG-40 has a higher dominant frequency than that of the sledgehammer. In both cases, the frequency was limited to the highest amplitudes for the processing.

4.2. QC Data Issues

During the QC analysis, some issues were detected in the data:

- Some data was affected by low frequency resonance depredating velocity spectrum and, therefore, making the dispersion curve picking impossible. This issue is identified in:
  - Shots 10010 and 10022 of L3 (Figure 14 – a) and b) respectively);
  - Shot 10052 of L8 (Figure 14 – c).
- Some shots were also affected by the plate's vibration, due to the coupling of the base plate to a hard surface, leading to a rebound of the base plate and causing subsidiary pulses and ringing effects:
  - Shot 10010 of L11 presents high frequency noise; therefore, this profile was processed in MASW using the maximum frequency content of 50 Hz (Figure 14 – d));
  - Shot 10026 of L13 was not processed in MASW because it shows multiple pulses caused by the plate's vibration (Figure 14 – e)).

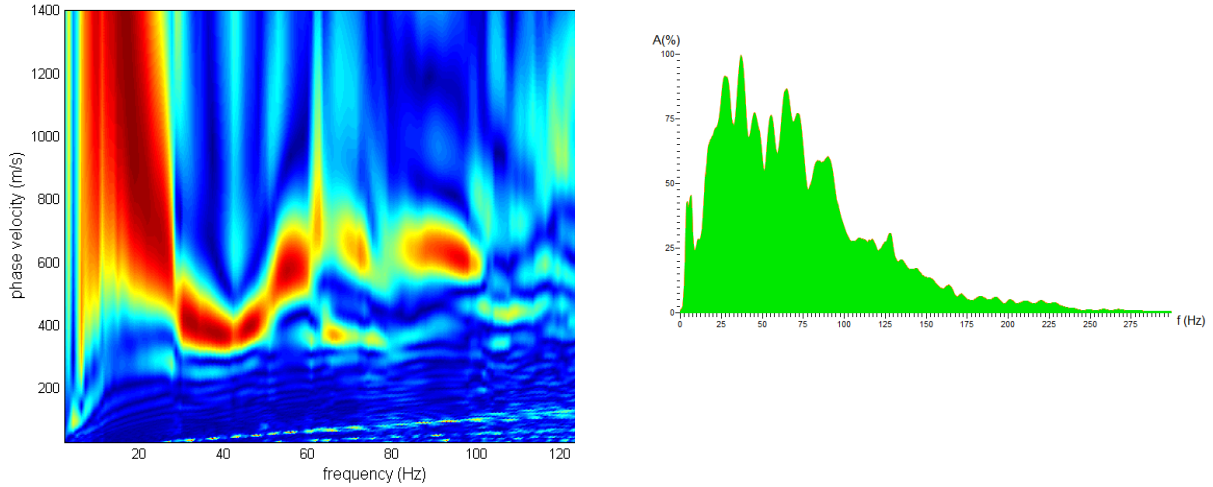
phase velocity (m/s)
frequency (Hz)
A(%)
f (Hz)

(a)

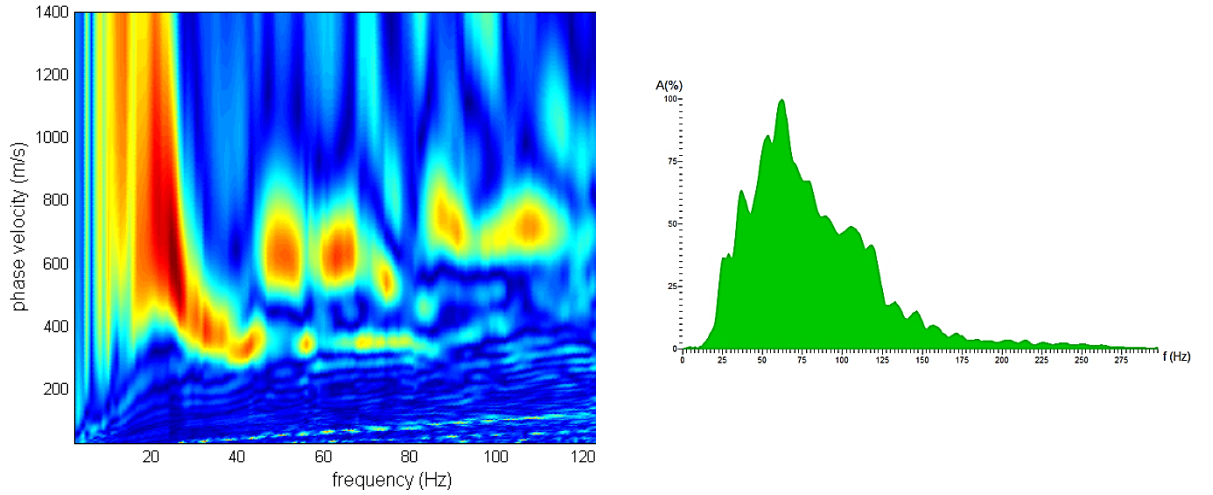
phase velocity (m/s)
frequency (Hz)
A(%)
f (Hz)

(b)

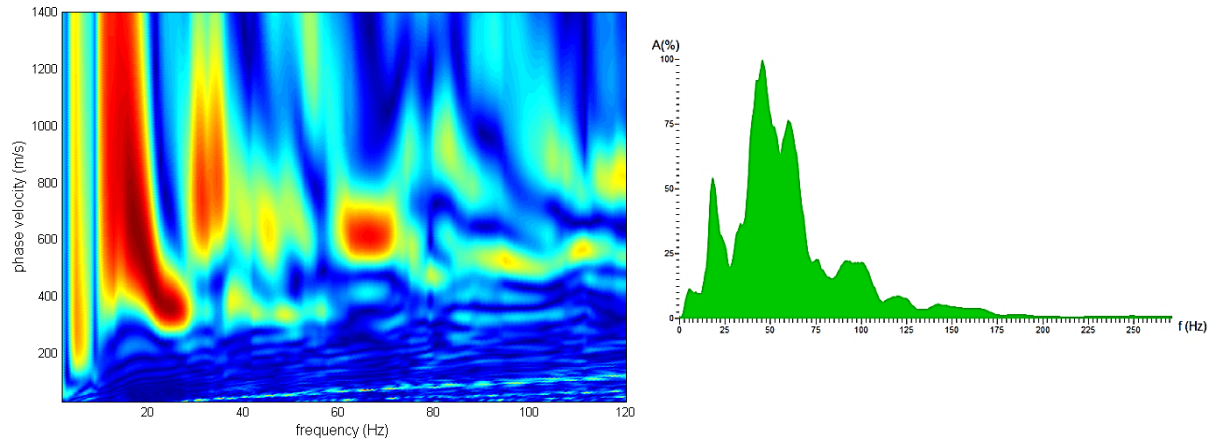
phase velocity (m/s)
frequency (Hz)
A(%)
f (Hz)

(c)

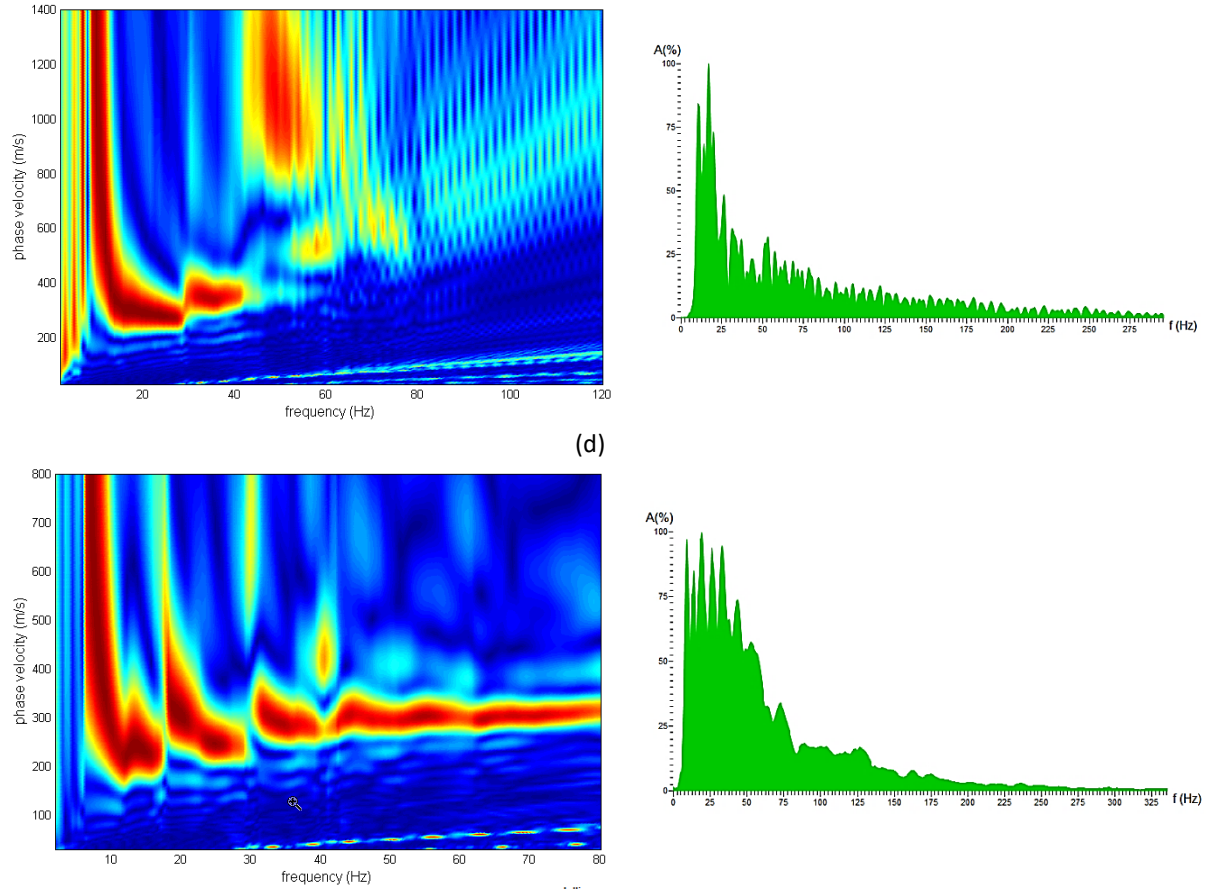

Figure 14 – Phase velocity spectrum on the left and frequency spectrum on the right for a) L3 shot 10010; b) L3 shot 10022; c) L8 and shot 10052; d) L11 and shot 10010 and e) L13 and shot 10026.

5. SEISMIC DATA PROCESSING

Twenty-eight seismic profiles were processed using MASW and refraction methodologies were used, respectively, winMASW® and Rayfract® software. The generic processing flow applied to the data was organized as in Figure 15. All the shots were used in the refraction methodologies, whereas, in the MASW, only the far offset shots were processed.

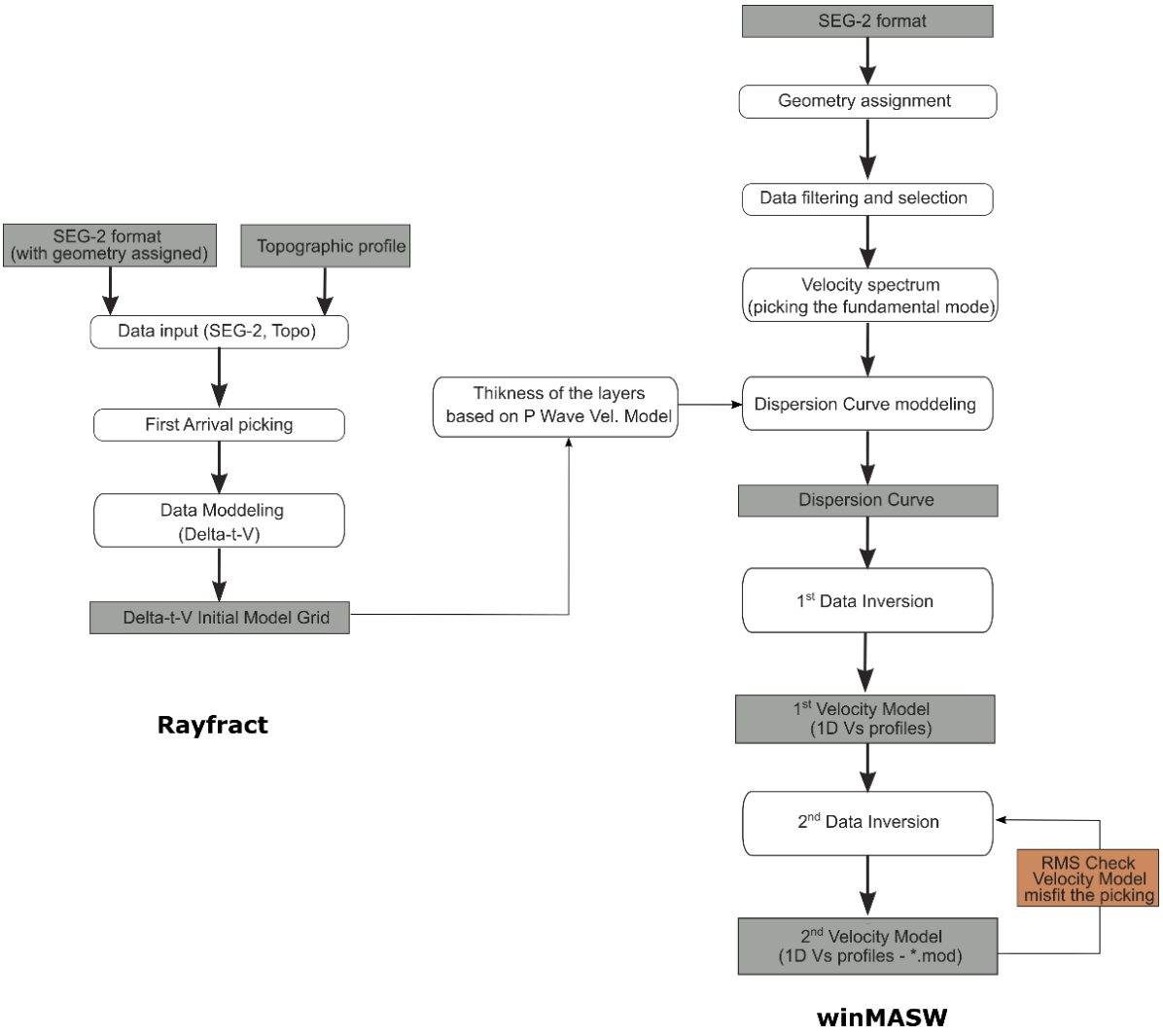

Figure 15 - Processing workflow applied to the seismic lines. Rounded boxes represent the processing steps and grey boxes represent the input/output products.

The use of the refraction processing was crucial for the MASW processing, because without an *a priori* processing to establish near surface structure (velocity and thickness), the dispersion of the results after inversion was tremendous.

5.1. Refraction Processing

The seismic refraction processing was done using Rayfract® software after importing the following data (Figure 15):

- SEG-2 with nominal geometry assigned;
- Topographic insertion.

The processing in Rayfract® included the picking of the first arrival (Figure 16), for every shot and every channel where the SNR allows accurate picking.
The analyses of the first arrival picking was done for every line, allowing a minimal RMS error of the Rayfract models (see Appendix A: Notation used)

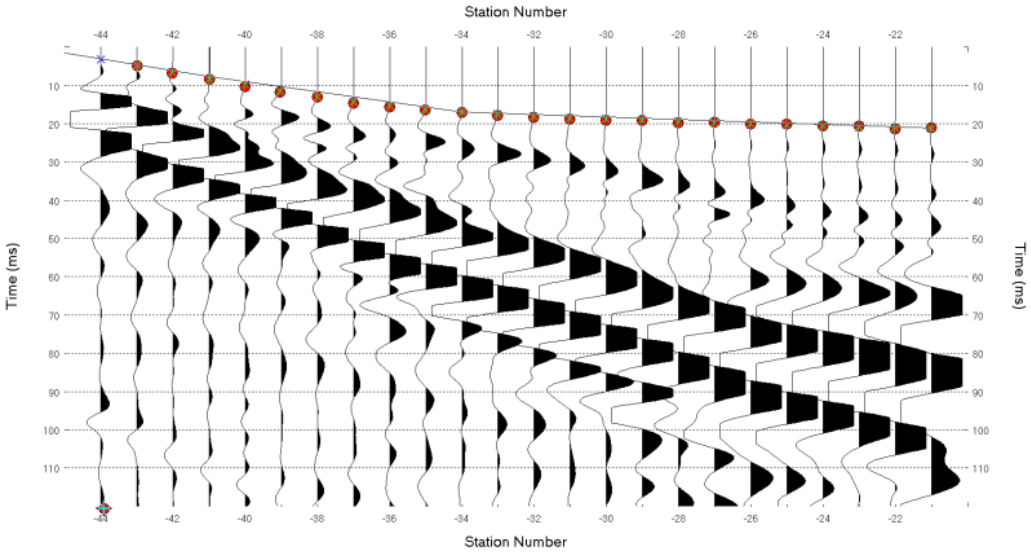

Figure 16– Shot gathered analysis (shot 10010, l01) for refracted wave analysis.

A 2D compressional wave velocity model in grid format (*.grd) was obtained for each line plotted using the ***Golden Software's Surfer®*** (see Figure 17, using the Delta-t-V method. This pseudo-2D turning ray inversion method was chosen because it delivers continuous 1D depth V_S. velocity profiles for all profile stations and it has a better vertical resolution than the other inversion methods available in the software.
The 2D compressional wave models were used to infer the thickness/geometry of the layers, as preliminary input for MASW data processing/modeling (see Figure 18).

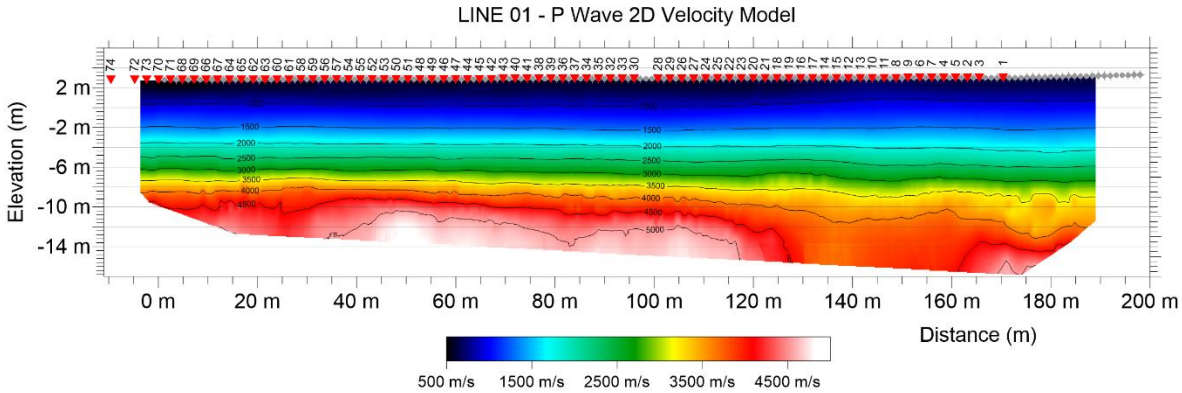

Figure 17 - 2D compressional wave velocity model obtained fom L01.MASW Processing

For each shotpoint with 9.6 m S/R offset, a 1D V_S vertical velocity model was located in the middle of the spread between the 12th and the 13th geophone (see red star in Figure 9). The source offset of 2.4m wasn´t used because it would not cover the desired investigation depth.

5.1.1. Model Creation

Since the objective is to characterize the landfill, the upper velocity limit of the 2D compressional wave velocity model was defined at $V_{P=}3500\ ms^{-1}$ for each line. The lower limit wasn´t standard because the V_{Pmin} was different for each model. However, the thicknesses of each layer h range were around 500 ms^{-1} (see Figure 18) in order to establish the surface layers of the 1D V_S vertical velocity model.

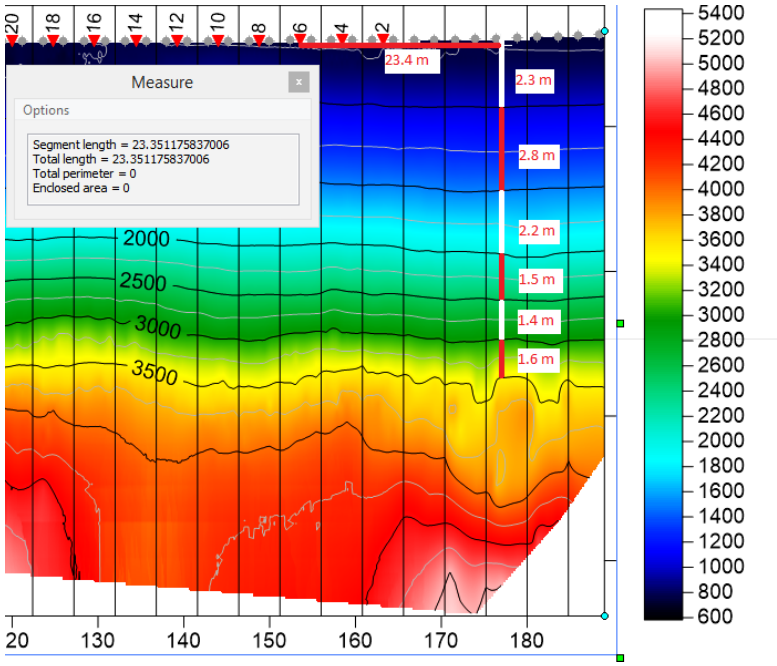

Figure 18 - Initial thickness model created for shot 10006 of L01. Note that the representative point for each shot is located 23.4 m from the shot's position, as exemplified in Figure 9.

Table 4- Thickness model used for shot 10006

$V_P\ (ms^{-1})$	$h\ (m)$
- 500	2.3
500 - 1000	2.8
1000 - 1500	2.2
1500 - 2000	1.5
2500 - 3000	1.4
3000 - 3500	1.6
3500 -	∞

5.1.2. Velocity Spectrum and dispersion curve picking

For each shot, superficial waves were selected (Figure 19) to represent the velocity spectrum.

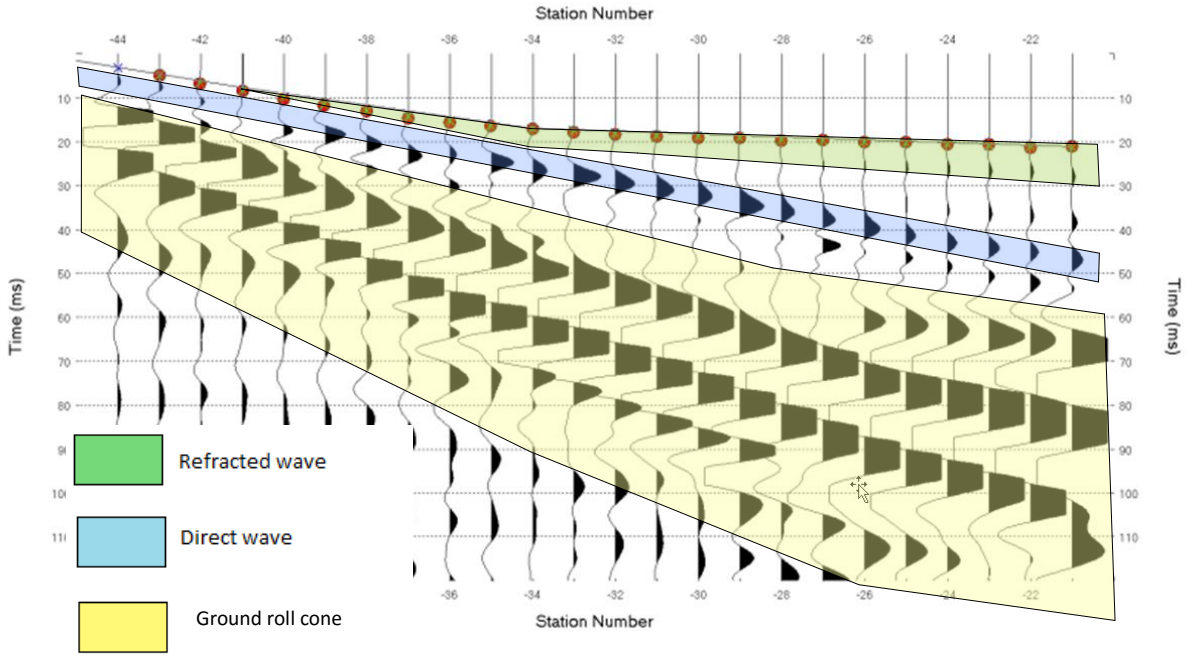

Figure 19 - Shot gathered analysis (shot 10010, l01) for refracted wave analysis - selection of the surface waves.

The velocity spectrum corresponds to an energy scatter plot that relates the frequency with the phase velocity for surface waves.

For picking the dispersion curve, the points that belonged to a particular propagation mode of a surface wave were selected and the fundamental mode (Figure 20) was picked in the f-v domain. Sometimes, the interference of different modes can alter the apparent dispersion characteristics of the fundamental mode or result in higher modes being misinterpreted as fundamental. Therefore, the picking was only made up until the interference of a higher mode.

All the 1D shear wave models resulted from the fundamental vibration mode picking of the velocity spectrum. Besides that, sometimes, a higher mode can be visible in the data such as in Figure 20, yet it wasn't consistent in all data.

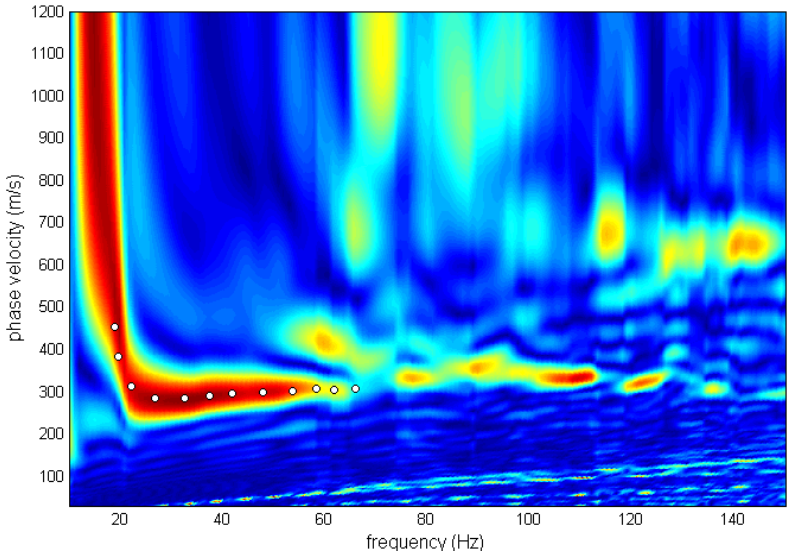

Figure 20 –Picking of the fundamental vibration mode – dispersion curve in the F-V domain.

After the picking in the f-v domain, it is possible to see the dispersion curve in the f-k spectrum (Figure 21).

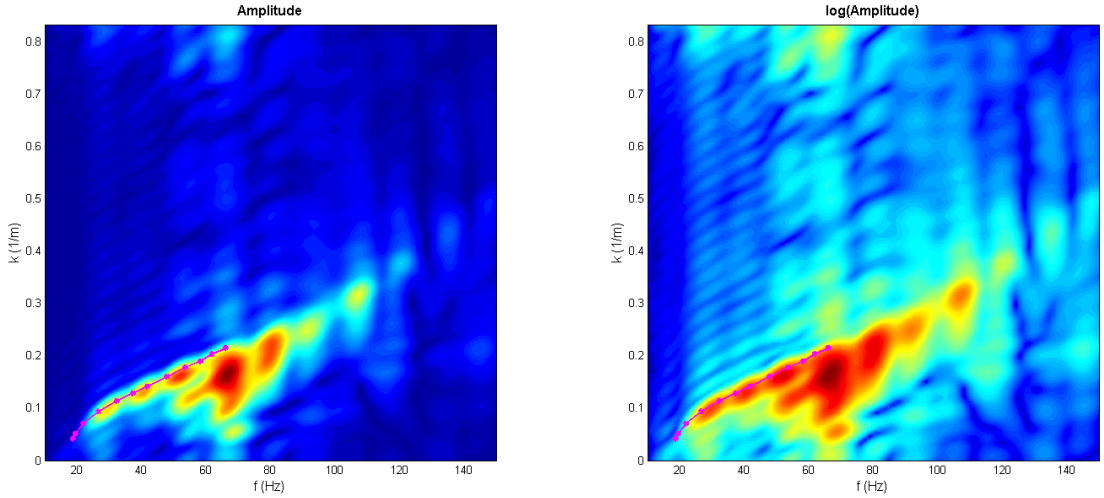

(a) *(b)*

Figure 21- Dispersion curve in the f-k spectrum: (a) amplitude and (b) logarithm of the amplitude.

5.1.3. Maximum depth penetration

The maximum penetration depth in a homogeneous medium is about one wavelength. The currently accepted rule of thumb for the maximum penetration depth is approximately half of the longest wave length (λ/2) or (λ/2.5) [Elisoft – geophysical software and services, 2015]. This value is the outcome of the relationship between velocity and the frequencies represented in the dispersion curve:

$$\lambda = \frac{V_f}{f}$$

Table 5 *- Relation between wave length and maximum depth penetration, relatively to the dispersion curve of shot 10006 of L01 (see* ***Figure 20****)*

F (Hz)	Vf (m/s)	λ (m)	Depth (m)	
19.484	395.000	20.273	8.109	10.136
20.649	352.370	17.065	6.826	8.532
22.719	317.599	13.980	5.592	6.990
26.729	295.272	11.047	4.419	5.523
31.387	289.546	9.225	3.690	4.613
35.915	290.107	8.078	3.231	4.039
40.185	292.611	7.282	2.913	3.641
44.584	295.915	6.637	2.655	3.319
48.853	299.264	6.126	2.450	3.063
52.476	301.971	5.754	2.302	2.877
55.839	304.226	5.448	2.179	2.724
59.203	306.081	5.170	2.068	2.585

In this particular shot, the maximum penetration depth was approximately 10 m.

5.1.4. Modeling and Inversion of the dispersion curve

The initial thickness model created, based on the refractive method, is introduced at this stage of processing (Figure 18), and then adjusted to the velocities of each layer and bedrock to adjust to the velocity spectrum (Figure 22).

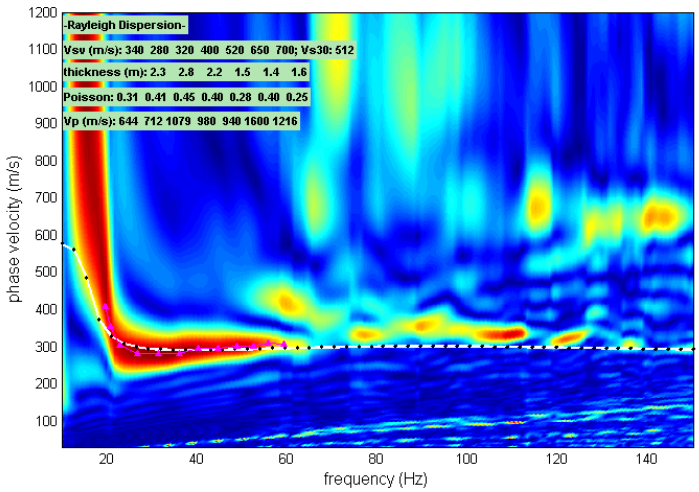

Figure 22 – Introduction of the initial thicknesses model based on the refraction method.

Table 6- Initial V_s profile used for shot 10006

$V_s\ (ms^{-1})$	$h\ (m)$
340	2.3
280	2.8
320	2.2
400	1.5
520	1.4
650	1.6
700	∞

Having finalized the adjustments of the model to the dispersion curve, the second phase was the inversion of the model created. This inversion is made by means of an optimization process (genetic algorithms) that requires the computer a big calculation effort. (Dal Moro et all, 2007)

In the inversion, two 1D V_S models were obtained: the "best" model (in terms of lower misfit, i.e the discrepancy between the observed and the calculated curve) and a medium model calculated by means of MPPD (*Marginal Posterior Probability Density)*. However, just the best model was considered further on. The next figure shows the results of the first inversion. (Figure 23)

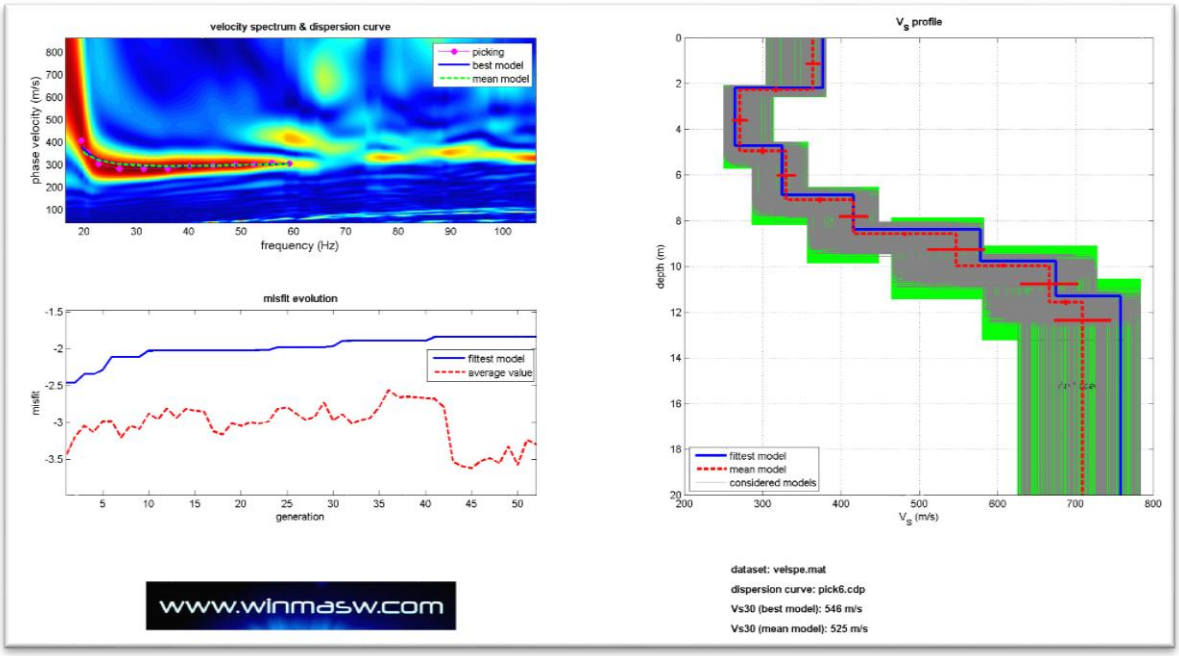

Figure 23 –First inversion results: Velocity spectrum and dispersion curve (a); misfit evolution (b); and 1D shear wave velocity model obtained for L1 for shot 10006.

To improve the results, namely the misfit evolution of the model to the velocity spectrum, a second inversion was made with the best output of the first inversion – the best model. In this inversion, its limits were adjusted to achieve a better approximation with the dispersion curve.
The next figure shows the results of the second inversion. (Figure 24)

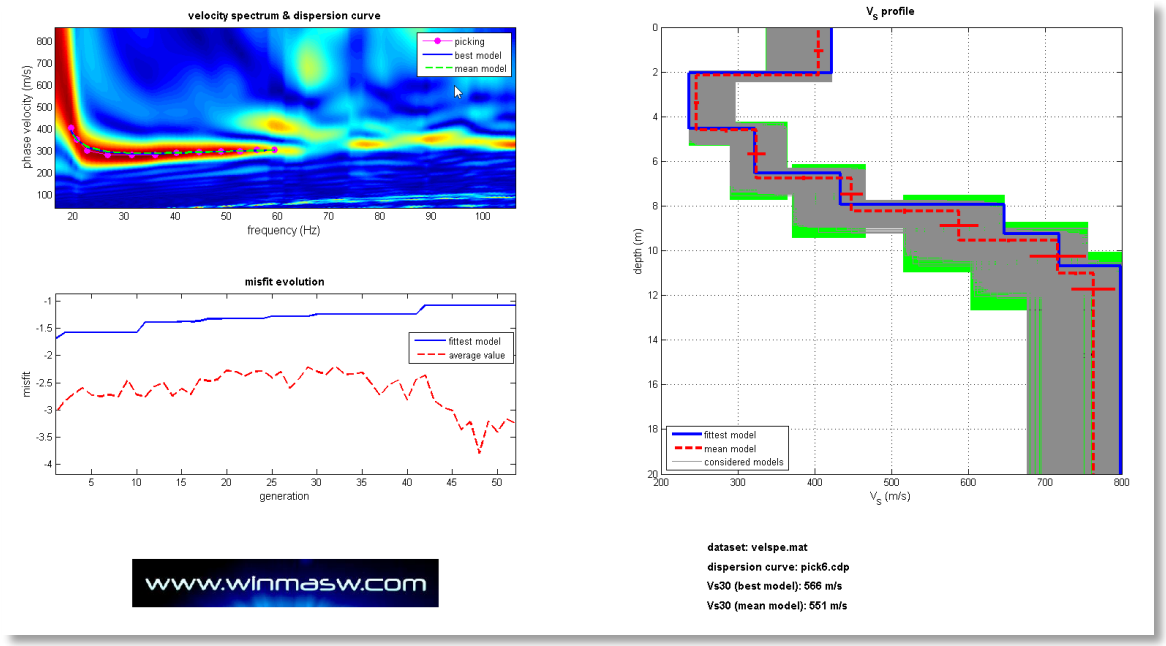

Figure 24 –Second inversion results: Velocity spectrum and dispersion curve (a); misfit evolution (b); and 1D shear wave velocity model obtained for L1 for shot 10006.

As it was expected, the error decreases, reaching a “misfit evolution" of 1% between the “fittest model” and the dispersion curve.

5.1.5. Model Validation

The 1D shear wave velocity model obtained in the second inversion must be compared with the dispersion curve of the fundamental mode in order to determine if the misfit is satisfactory (Figure 25).

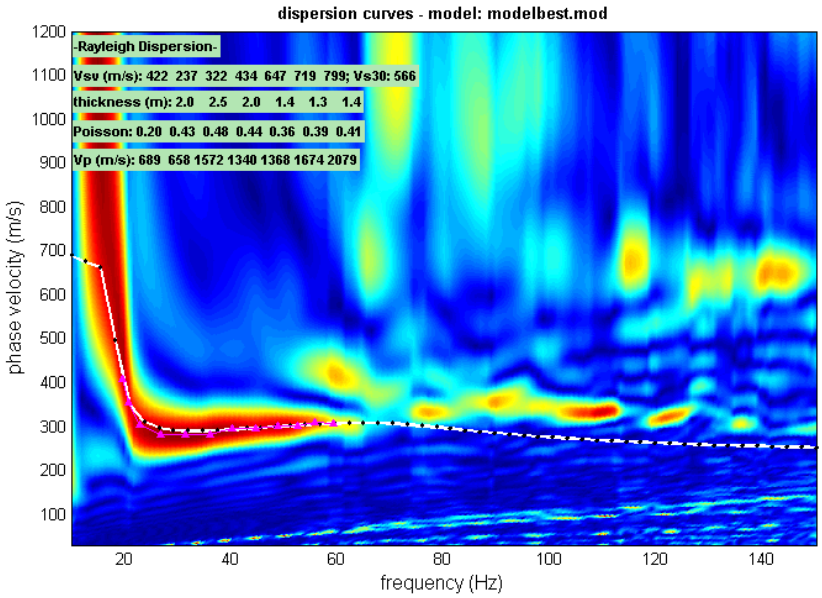

Figure 25– Comparison between the dispersion curve and the final model created

For the interpolation, each and every S-wave profile (V_S versus depth) was displaced/ incremented with its respective topographic elevation, as represented in Figure 26. Also, the layer thickness, given by the software winMASW®, was converted to the depth of half of the layer, considering 2 points for the first layer (1/2 layer and the topography), both with the same velocity and a middle point for the remaining layers (see example in Figure 26).

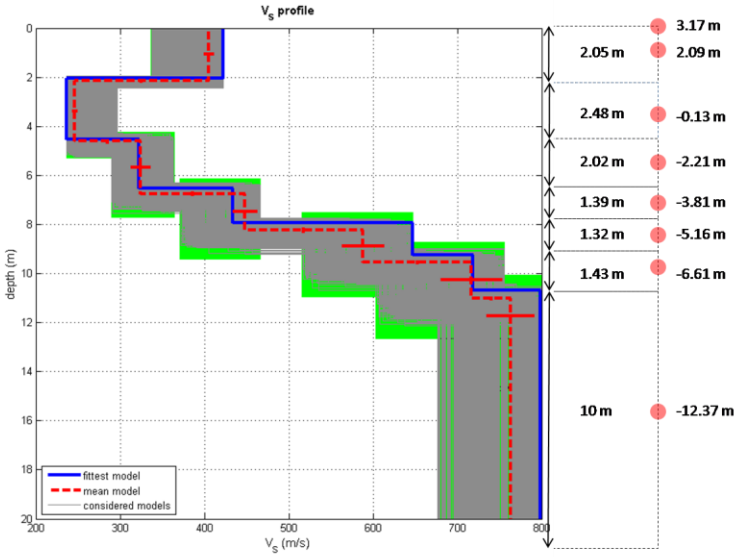

Figure 26– Example of a conversion from layer thickness given by the 1D model to the depth of half a layer used to generate the 2D shear wave velocity models.

To generate a 2D V_S section, all 1D V_S models per line are interpolated and plotted using Golden Software's Surfer®

6. RESULTS AND DISCUSSION

The 2D shear wave velocity section was obtained for each profile using Golden Software's Surfer® and interpolating all 1D V_S models of the respective line (Figure 26). The interpolation was performed using the Triangulation methodology (Golden Software, Inc, 2014) with a spacing of 0.2 m and anisotropy ratio of 5. The model was filtered using a low pass filter (moving average) with a filter size of 3 rows x 5 columns.

The lines were plotted from southwest (SW) to northeast (NE), independently of the acquisition orientation.

For a better perception of the evolution of the dynamic properties of the soil along the landfill, all the 28 2D shear velocity models were paced in its locations and represented by a 3D software - Voxler 3® by Golden Software, on a representative scheme of the area under study.

In addition to that, every model has its own V_{S30} graphic on top, rightly placed. This value it's an output of the software winMASW for every 1D V_S profile. This estimation, however, goes beyond the maximum penetration depth, so after the layer stratification, the bedrock is assumed with the same shear wave velocity until the 30 m of depth.

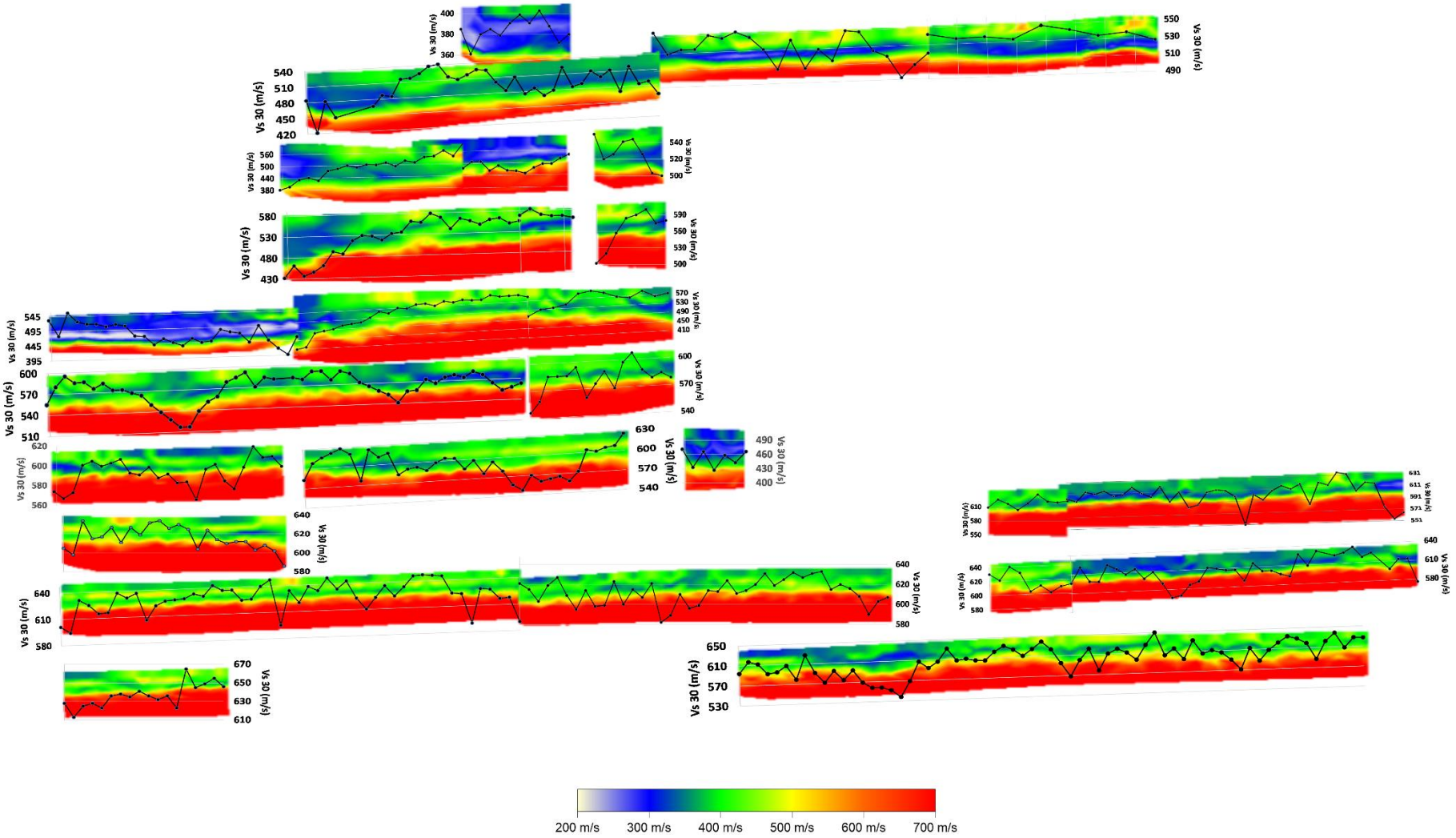

Figure 27– 3D map showing the shear wave velocity models for the study area.

Concerning the sea location, at northwest from the survey, it is possible to see the deepening of the bedrock towards the sea. However, the landfill is at the same height relative to the average level of the sea water due to the higher thickness of sediments above.

Regarding the acquisition time, the lines acquired in March (rainy season) (Table 3) present lower velocities above the bedrock, this is probably due to the high water content in the landfill in that time season. On the contrary, as expected, the remaing lines, in general, present higher velocities in the landfill. However, closest to the sea, the shear waves velocities models tend to decrease its velocities in the landfill, for example L04_B, L12_B, L12_A, etc. (Figure 6 and Figure 27).

Besides, several elements may affect the shear wave's velocities, such as tides, uneven compression in the landfill, different soils, which can lead to different elastic properties, etc.

A deeper analysis could be done to each shear wave velocity model, so three profiles were chosen to compare L01, L02 and L06 (Figure 28 and Figure 29-b)).

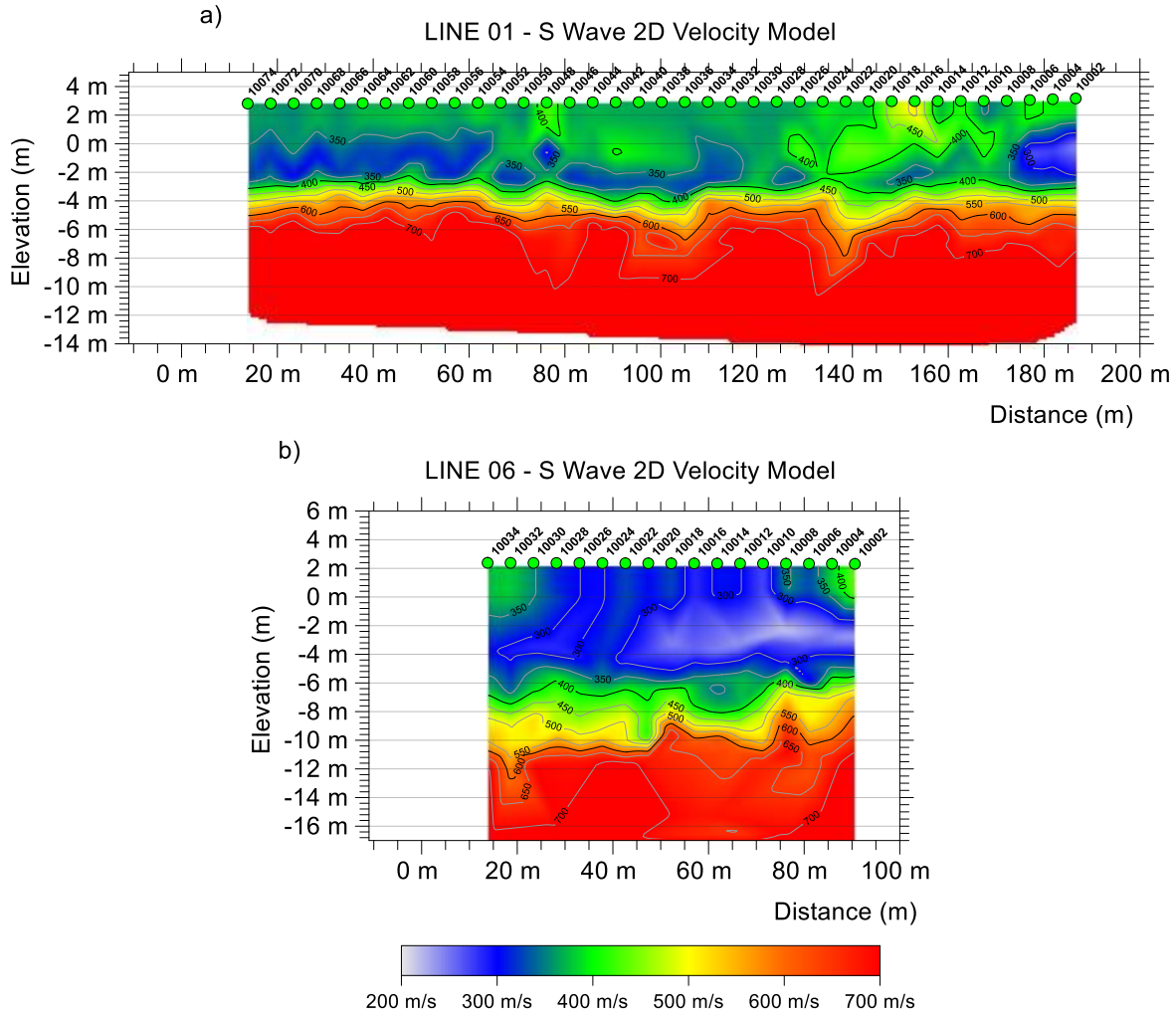

Figure 28–shear wave velocity model for a) L01 and b) L06 resultant from the interpolation of all 1D V_S models obtained for each line.

The purpose of comparing L01 and L06 is to understand the influence of different compaction energies (Figure 5) on shear wave velocities. For that effect, the lines were acquired in the same season to eliminate other factor influences.
Analyzing these two models, the differences in the depth of the bedrock is clearly visible, changing approximately 5 m. The minimum shear wave velocity achieved in both models is not significant. In model 06, $V_{Smin} = 217\ m/s$ where as in model 01, $V_{Smin} = 245\ m/s$.
However, despite the L06 being acquired in a zone with higher compaction energy (7000-8000 kNm) than the L01 (6000 kNm), the shear wave velocities in L06 are lower than in L01. Perhaps the proximity of the sea may have a greater influence than the compaction energy made on site or the materials used in each section of the landfill were different, having consequently a different responses.
The purpose of comparing L01 and L02 is to understand the influence of the rainy season in the landfill behavior. Comparing this two models, the minimum velocity in L01, as it was already said above, is $V_{Smin} = 245\ m/s$, where as in model 02, $V_{Smin} = 293\ m/s$. The lines acquired in June reveals higher minimum velocities (almost $50 m/s$) than the one acquired in March, even though L01 being located in a bigger energy compaction zone.

6.1. V_{S30} Analysis

All the lines analyzed present a V_{S30} above 360 m/s, which means that, by Caltrans Seismic Design Criteria, all the soils are considered in the site class C - Very dense soil and soft rock.
However, there are some diferences between the lines. For instance, there are models with very low values for the V_{S30}, such as L04_B, L10, L11 and L13 and models with a great variety, like L02 or L07_B. Althought, the lack of information regarding the site, namely the soil conditions and composition prevent a deeper analysis.

6.2. Tides Influence

Finally, to exemplify the tides influence in the shear wave velocities models, due to the water level variation, I used L02 to make this analysis because it was acquired in two different days.
Analyzing the log acquisition of this line (Table 7), regarding the day and hour, a tides plot for each day was taken and plotted (Figure 34). These tides plots relate the sea level, in meters, with the time of the day, indicating also the high and low tides periods.
For a better visualization and characterization, the tides plot were edited and selected for the acquisition period of each shot (Figure 29).

Table 7 - Acquisition log for L02

Station	File name	Date	Hour
-8	10002	1st acq. day	2:02
-12	10004	1st acq. day	2:09
-16	10006	1st acq. day	2:16
-20	10008	1st acq. day	2:21
-24	10010	1st acq. day	2:25
-28	10012	1st acq. day	2:30
-32	10014	1st acq. day	2:38
-36	10016	1st acq. day	2:43
-40	10018	1st acq. day	2:48
-44	10020	1st acq. day	2:54
-48	10022	1st acq. day	3:04
-52	10024	1st acq. day	3:08
-56	10026	1st acq. day	3:14
-60	10028	1st acq. day	3:20
-64	10030	1st acq. day	3:24
-68	10032	1st acq. day	3:29
-72	10034	1st acq. day	3:34
-76	10036	1st acq. day	3:37
-80	10038	1st acq. day	3:43
-84	10040	1st acq. day	4:53
-88	10042	1st acq. day	5:00
-92	10044	1st acq. day	5:12
-96	10046	1st acq. day	5:16
-100	10048	1st acq. day	5:22
-104	10050	1st acq. day	5:26
-108	10052	1st acq. day	5:32
-112	10054	1st acq. day	5:36
-116	10056	1st acq. day	5:45
-120	10058	1st acq. day	5:55
-124	10060	1st acq. day	6:01
-128	10062	2nd acq. day	2:30
-132	10064	2nd acq. day	2:35
-136	10066	2nd acq. day	2:39
-140	10068	2nd acq. day	2:43
-144	10070	2nd acq. day	2:47
-148	10072	2nd acq. day	2:51
-152	10074	2nd acq. day	2:54
-156	10076	2nd acq. day	2:59
-160	10078	2nd acq. day	3:09
-164	10080	2nd acq. day	3:12
-168	10082	2nd acq. day	3:16
-172	10084	2nd acq. day	3:30
-176	10086	2nd acq. day	3:34
-180	10088	2nd acq. day	3:37
-184	10090	2nd acq. day	3:42
-188	10092	2nd acq. day	3:48
-192	10094	2nd acq. day	3:51
-196	10096	2nd acq. day	3:54
-200	10098	2nd acq. day	3:58
-204	10100	2nd acq. day	4:01
-208	10102	2nd acq. day	4:04
-212	10104	2nd acq. day	4:10
-216	10106	2nd acq. day	4:23
-220	10108	2nd acq. day	4:26
-224	10110	2nd acq. day	4:30
-228	10112	2nd acq. day	4:34
-232	10114	2nd acq. day	4:38
-236	10116	2nd acq. day	4:41
-240	10118	2nd acq. day	4:48
-244	10120	2nd acq. day	5:08
-248	10122	2nd acq. day	5:14
-252	10124	2nd acq. day	5:17
-256	10126	2nd acq. day	5:25
-260	10128	2nd acq. day	5:28
-264	10130	2nd acq. day	5:31
-268	10132	2nd acq. day	5:35
-272	10134	2nd acq. day	5:38

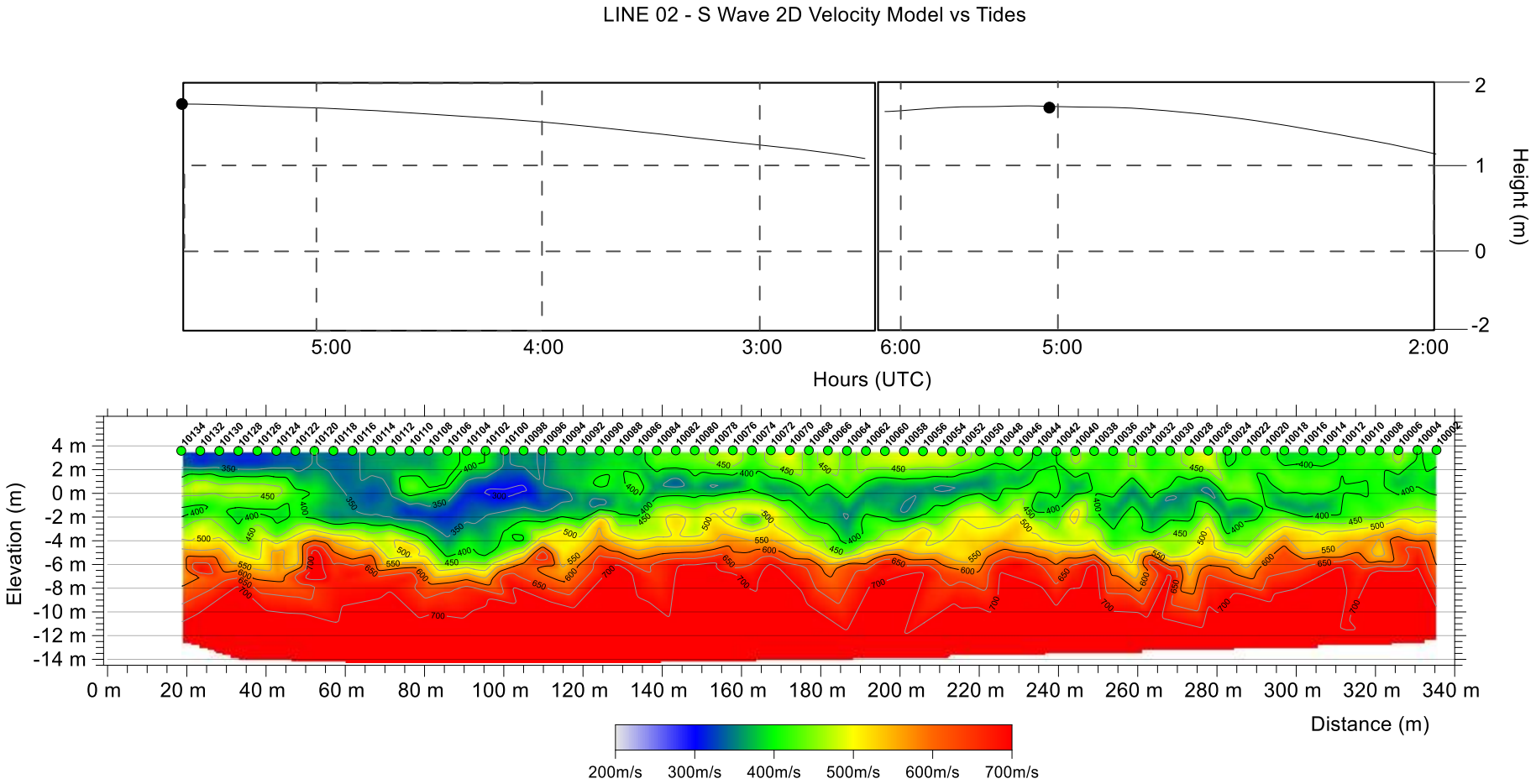

Figure 29 - Tides plot (above) regarding the acquisition time of the shots. Note that the line's acquisition begins on the right side (1st Acquisition day); after the shot 10060, the line was acquired in the second day, having a different tides plot.

As we can see the tides level has a real impact in the shear wave velocity model, a lower velocity layer follows the tides level along the line, reaching a maximum elevation in the highest tides, in both days. Furthermore, the differences in tides level is visible in the shear wave's velocity (transition between shots 10060 and 10062). However, the differences in the tides only change the saturation level, because a higher zone still affected with water.

6.3. Elastic Modulus

[Mavko, G. *et al*, 2009] summarizes some popular and useful $V_P - \rho$. Density is a simple volumetric average of the rock constituent densities and is closely related to porosity by:

$$\rho_b = (1 - \phi)\rho_0 + \rho_{f1}$$

where ρ_0 is the density of mineral grains, ρ_{f1} is the density of pore fluids, and ϕ is the porosity.

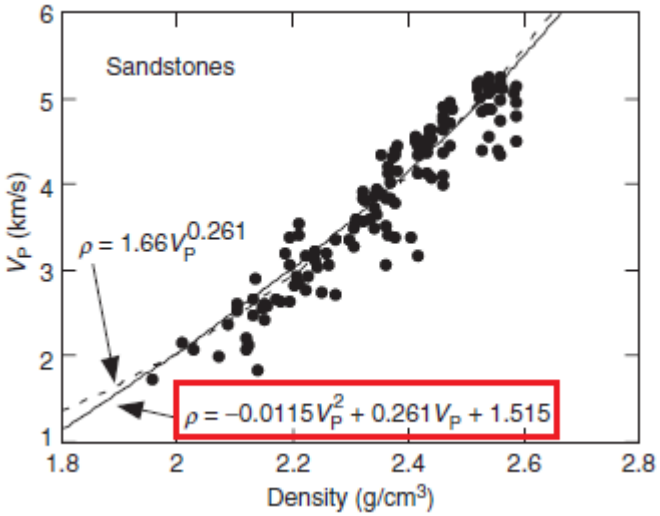

Figure 30 - Both forms of Gardner's relations applied to log and laboratory sandstone data- [Castagna et al., 1993]

Using the equation selected in red, it was possible to estimate the density from the P-wave models. However, this was only an estimation, because the equation is intended for consolidated rocks, wich is not the case of landfill in study. Above it is the result of the density model calculation using the equation referred.

The following profiles (Figure 31 & Figure 32) were disposed with a vertical scale of 1:15 and a horizontal scale of 1:30.

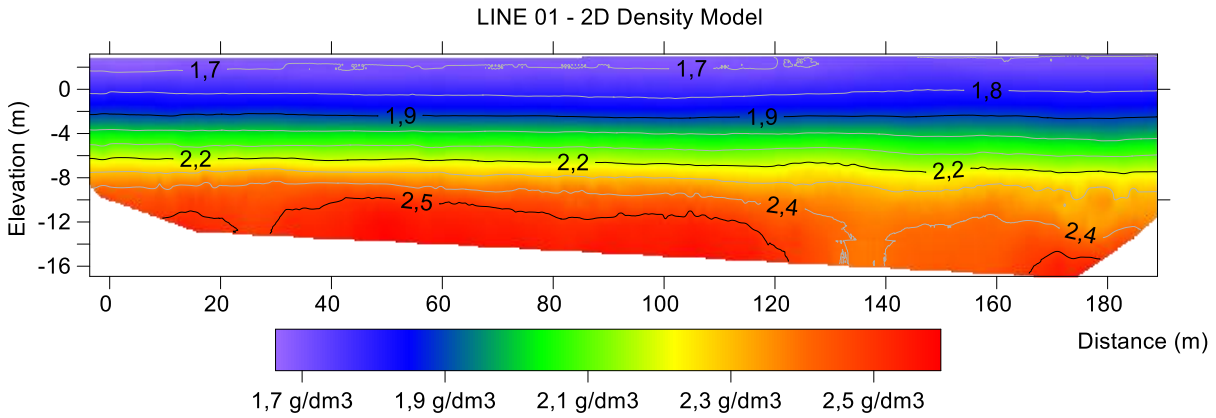

Figure 31 – 2D Density model calculated to L01 from the 2D P-wave velocity model of the same profile.

With the density values calculate, it is already possible to achieve the shear modulus (Figure 32), through the formula: $G_{max} = \rho {V_S}^2$. However, due to the high uncertainties and approximate equations, this is only an example, not being calculated for all profiles performed in the landfill.

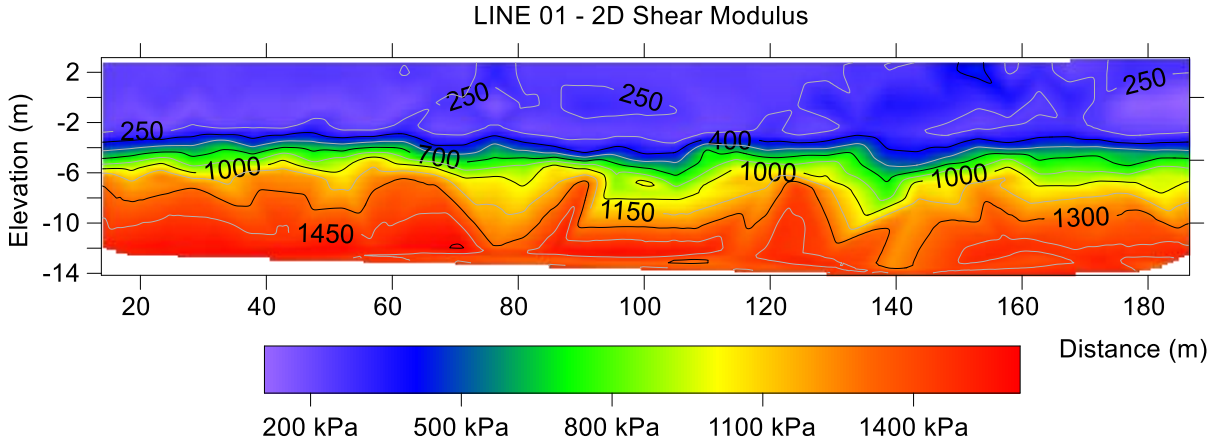

Figure 32- 2D Shear modulus calculated to L01 from the 2D S-wave velocity model and the density model of the same profile

7. CONCLUSIONS

The construction landfill was successfully surveyed. The site was acoustically very noisy; nevertheless, due to the decision of acquiring data during the night shift, the obtained data shows high quality level allowing a reliable interpretation for refraction method and for surface waves analysis.

In seismic refraction, 1396 shots were analyzed, resulting in 28 2D compressional velocity models, making a total length of 4267 m. For MASW, 695 shots were analyzed, resulting in 695 1D shear velocity profiles and 28 2D models, making a total length of 3225 m.

The quality control and acquisition format, provided by Geosurveys, was tailored to ensure that the acquired data meet the requirements, in order to better estimate the seismic wave velocities and, therefore, to assess the elastic condition of the landfill. The acquisition parameters, namely the number of geophones, the distance between them and the use of the biggest shot offset allow a better vertical and horizontal resolution, however a horizontal resolution of 4.8 m in the 2D shear wave velocity model is relatively low.

The obtained shear wave velocity models are in agreement with the site characteristics, according to the information available. Within the same line, the 1D shear wave velocity profiles show a good lateral continuity and consistency in velocity variations, with velocities varying between 200 and 500m/s within the landfill. A shear wave velocity inversion can be seen in almost the profiles (see Figure 27), from 0 m (MSL) until the bedrock, what is consistent with the phreatic level.

The landfill velocities (above the bedrock) obtained for the lines acquired in March are lower than the velocities obtained for the lines acquired in June, this is probably due to the high water content in the landfill in March (rainy season). At first sight, the different energy compaction zones did not have a direct and straight forward relation with the shear wave velocity models.

Regarding the V_{S30} analysis, all the lines present values above 360 m/s, which means that, by Caltrans Seismic Design Criteria, all the soils are considered in the site class C - Very dense soil and soft rock. However, there are some diferences between the lines. For instance, there are models with very low values for the V_{S30}, such as L04_B, L10, L11 and L13, that could have a different site response comparatively to the other models.

For future work, a couple of cross sections models could be acquired in order to evaluate the landfill behavior along the coast. Some field testes, after the final compaction and construction of the landfill, such as drilling, SPT, sampling and laboratory testing could be useful to consolidate the work. Those would allow the comparison between the shear wave velocities and the SPT tests or an accurate evaluation of shear modulus, if some densities measures of the landfill where supplied.

REFRENCES

Akin, M. K., Kramer, S.L., Topal, T. (2011) "Empirical correlations of shear wave velocity (V_S) and penetration resistance (SPT-N) for different soils in an earthquake-prone area (Erbaa-Turkey)." *Engineering Geology*, pp. 1-17

Carvalho, J., Torres, L., Castro, R., Dias, R., and Mendes-Victor, L. (2009) "Seismic velocities and geotechnical data applied to the soil microzoning of western Algarve, Portugal." Journal *of Applied Geophysics*, pp. 249-258

Castagna, J.P., Batzle, M.L., and Kan, T.K., (1993). Rock physics – The link between rock properties and AVO response. In Offset-Dependent Reflectivity – Theory and Practice of AVO Analysis, ed. J.P. Castagna and M. Backus. Investigations in Geophysics, No. 8, Society of Exploration Geophysicists, Tulsa, Oklahoma, pp. 135–171.

Dal Moro, G., Pipan, M., Forte, E., Finetti, I. (2003) "Determination of Rayleigh wave dispersion curves for near surface applications in unconsolidated sediments." *Expanded Abstract, Society of Exploration Geophysicists"*, pp. 1247-1250.

Dal Moro G., Pipan M. & Gabrielli P., (2007), "Rayleigh Wave Dispersion Curve Inversion via Genetic Algorithms and Posterior Probability Density Evaluation", J. Appl. Geophysics, 61, 39-55

Das, B. M., (2010). Principles of Geotechnical engineering, (7th Edition). CL Engineering, 114-152

Elisoft – geophysical software and services (2015). WinMASW 7.0 User manual

Golden Software, Inc 2014. SURFER User's Guide. Golden, CO: Golden Software. pp.273

Hanumantharao, C., and Ramana, G. V. (2008) "Dynamic soil properties for microzonation of Delhi, India." *J. Earth Syst Sci 177, S2*, pp. 719-730

LAY, T. & WALLACE, T.C. (1995), "Modern Global Seismology", Academic Press

Lopes, I., Deidda, G.P., Mendes, M., Strobbia, and C., Santos, J. (2013) "Contribution of in situ geophysical methods for the definition of São Sebastião crater model (Azores)." *Journal of Applied Geophysics"*, pp. 265-279

Maheswari, R. U., Boominathan, A., Dodagoudar, G. R. (2010) "Use of Surface waves in Statistical Correlations of shear waves velocity and Penetration resistance of Chennai soils." *Geotech Geol Eng 28*, pp. 119-137

Mavko, G., Mukerji, T., Dvorkin, J. (2009). "The Rock Physics Handbook", (second Edition). Cambridge University press. Pp 380-382

Neves, S., Borges, J., Casacão, J., Caldeira, B. and Bezzeghould, M. (2014) "Near surface characterization of Faial island (Azores)." *8ª Assembleia Luso Espanhola de Geodesia e Geofisica*, pp. 138-147

Park, C.B., Miller, R.D., and Xia, J. (1998a) "Imaging dispersion curves of surface waves on multi-channel record." *68th Ann. Internat. Mtg. Soc. Expl. Geophys., Expanded Abstracts*, pp. 1377-1380.

Redpath, B.B., 1973, Seismic refraction exploration for engineering site investigations, Technical Report E-73-4, U.S. Army Engineering Waterways Experiment Station Explosive Excavation Research Laboratory, Livermore, California

Tselentis G-A And Delis G., 1998: Rapid Assessment Of S-Wave Profiles From The Inversion Of Multichannel Surfacewave Dispenion Data. An. Geophys., 41,1, 1-17.

Wair, B. R. & DeJong J. T. (2012). "Guidelines for Estimation of shear wave velocity profiles", PACIFIC EARTHQUAKE ENGINEERING RESEARCH CENTER, pp. 1-5

Xia, J., Miller, R.D., Park, C.B., Ivanov, J., Tian, G., Chen, C. (2004) "Utilization of high-frequency Rayleigh waves in near-surface geophysics." *The Leading Edge, 23(8)*, pp. 753-759. doi: 10.1190/1.1786895

Xia, J., Miller, R.D., and Park, C.B. (2000a) "Advantages of calculating shear-wave velocity from surface waves with higher modes." *[Exp. Abs.]: Soc. Expl. Geophys.,* pp. 1295-1298.

Xia, J., Miller, R.D., and Park, C.B. (1999) "Estimation of near-surface shear-wave velocity by inversion of Rayleigh waves." Geophysics, v. 64, n. 3, pp. 691-700.

Appendix A: Notation used

Table 8- Notation used

Symbol	Meaning	SI units
G_{max}	shear modulus	Pa
ρ	density	gcm^{-3}
V_S	Shear velocity	ms^{-1}
h	thickness of layers	m
f_i	frequency	Hz
c_{RJ} ou Vf	Rayleigh wave phase velocity	ms^{-1}
C	Compaction energy	$kN.m$
V_{Pmin}	P-wave minimum velocity	ms^{-1}
λ	Wave lenght	m
V_{Smin}	S-wave minimum velocity	ms^{-1}
E	Young modulus	Pa
θ	Poisson ratio	-
$V_{S,30}$	time-average shear wave velocity in the topmost 30 meters	ms^{-1}

Appendix B - Seismic Refraction Quality Control

Table 9 - Seismic Refraction QC for L01

EXAMPLE OF A SHOT	SHOT BREAKS
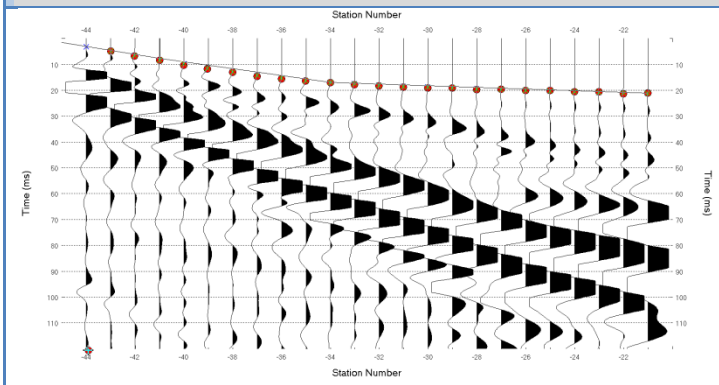	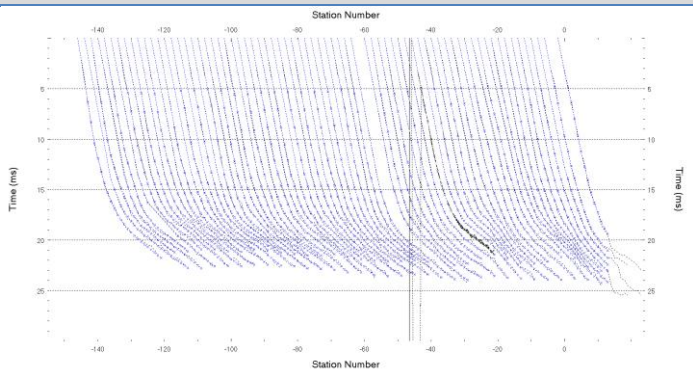

Goodness of Fit between modelled and picked traveltimes after 20 WET iterations :
RMS error : 0.17 millisecs.
Normalized RMS error : 0.7 percent (RMS error, divided by maximum pick time of all traces modelled)
Relative misfit function : 0.01 millisecs. (Gerard T. Schuster 1993 p. 1315; squared error summed over all traces modelled, divided by twice the modelled trace count)
# of traces modelled : 1652

Table 10 - Seismic Refraction QC for L02

EXAMPLE OF A SHOT	SHOT BREAKS
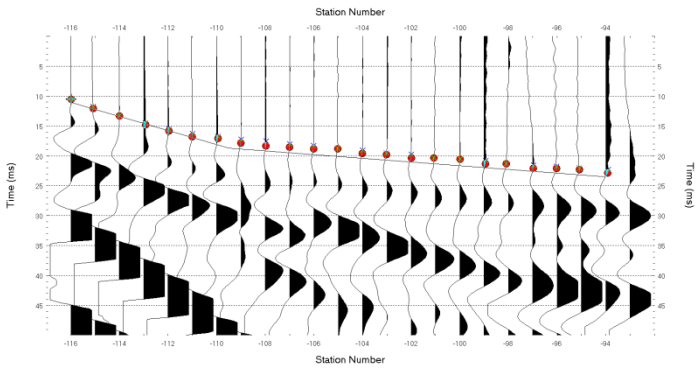	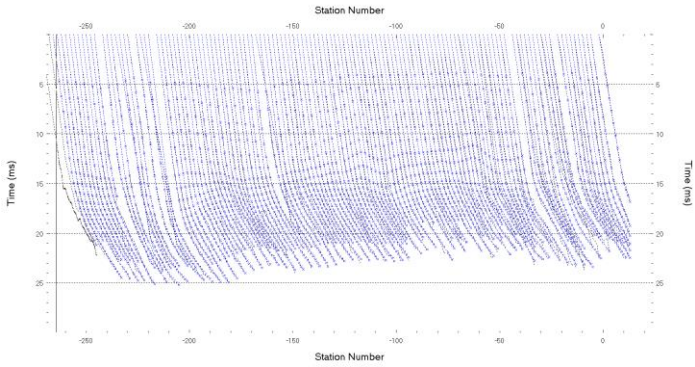

Goodness of Fit between modelled and picked traveltimes after 25 WET iterations :
RMS error : 0.30 millisecs.
Normalized RMS error : 1.2 percent (RMS error, divided by maximum pick time of all traces modelled)
Relative misfit function : 0.05 millisecs. (Gerard T. Schuster 1993 p. 1315; squared error summed over all traces modelled, divided by twice the modelled trace count)
# of traces modelled : 2818

Table 11-Seismic Refraction QC for L06

EXAMPLE OF A SHOT	SHOT BREAKS
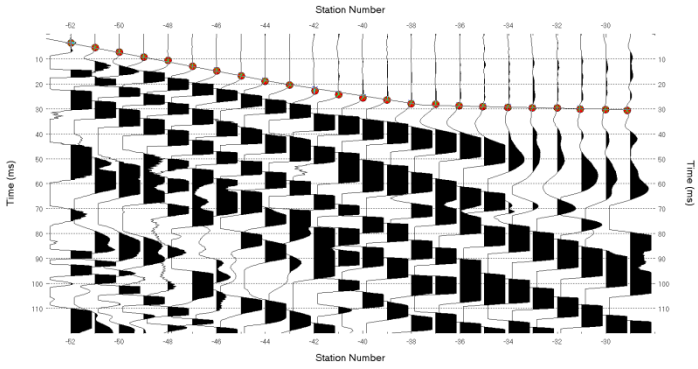	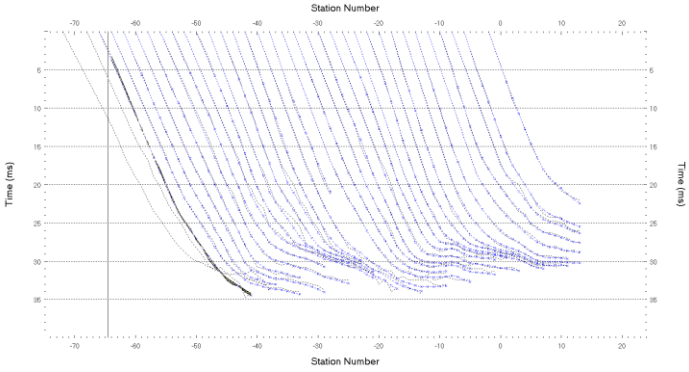

Goodness ofFit between modelled and picked traveltimes after 25 WET iterations :

RMS error : 0.29 millisecs.

Normalized RMS error : 0.8 percent (RMS error, divided by maximum pick time of all traces modelled)

Relative misfit function : 0.04 millisecs. (Gerard T. Schuster 1993 p. 1315; squared error summed over all traces modelled, divided by twice the modelled trace count)

Maximum absolute error : 1.28 millisecs., for trace 022-008 (Shot#-Trace#)

# of traces modelled : 700

Appendix C - 2D compressional wave velocity model

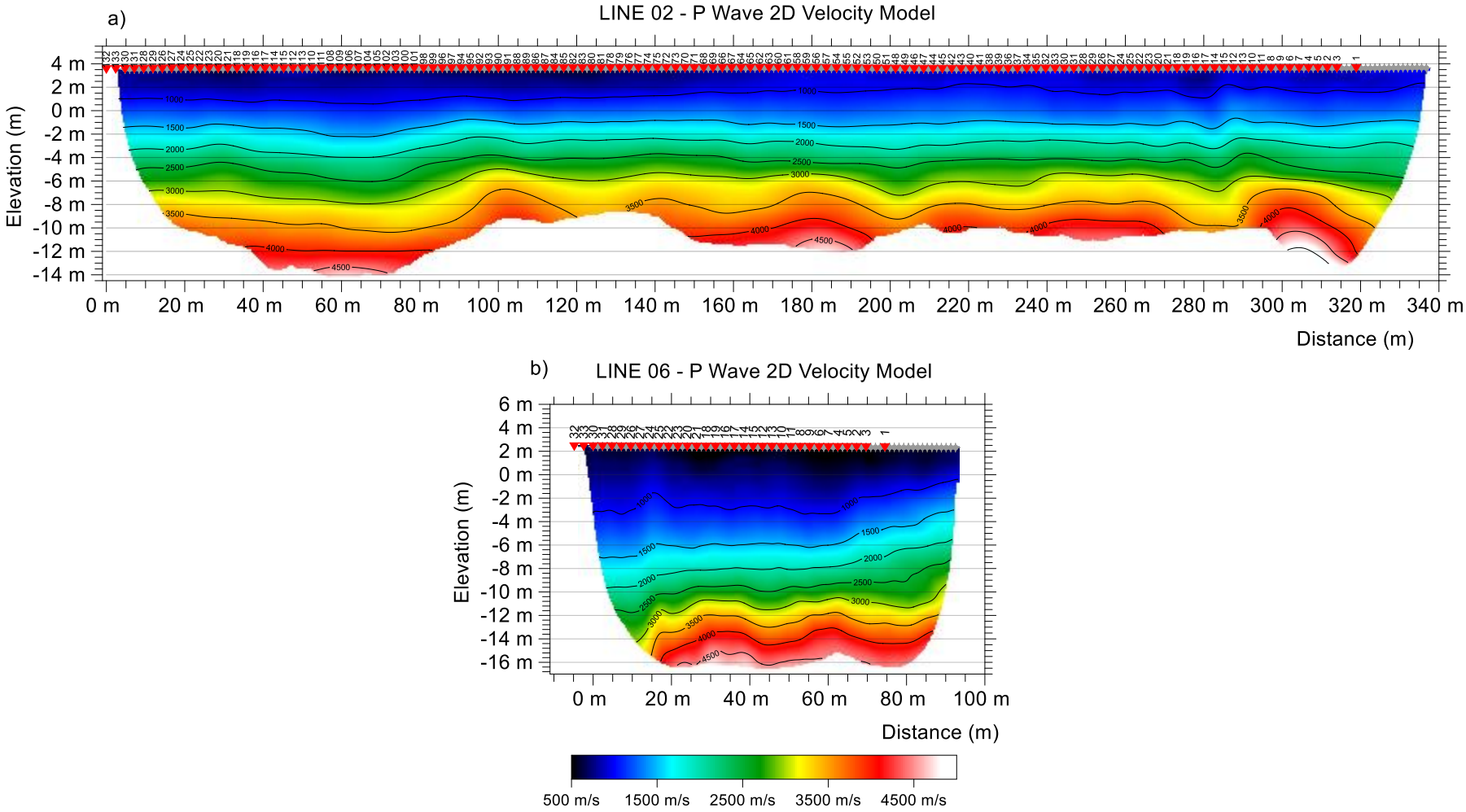

Figure 33- 2D compressional wave velocity model obtained for a) L02 and b) L06.

Appendix D - Tides plot for L02's acquisition days

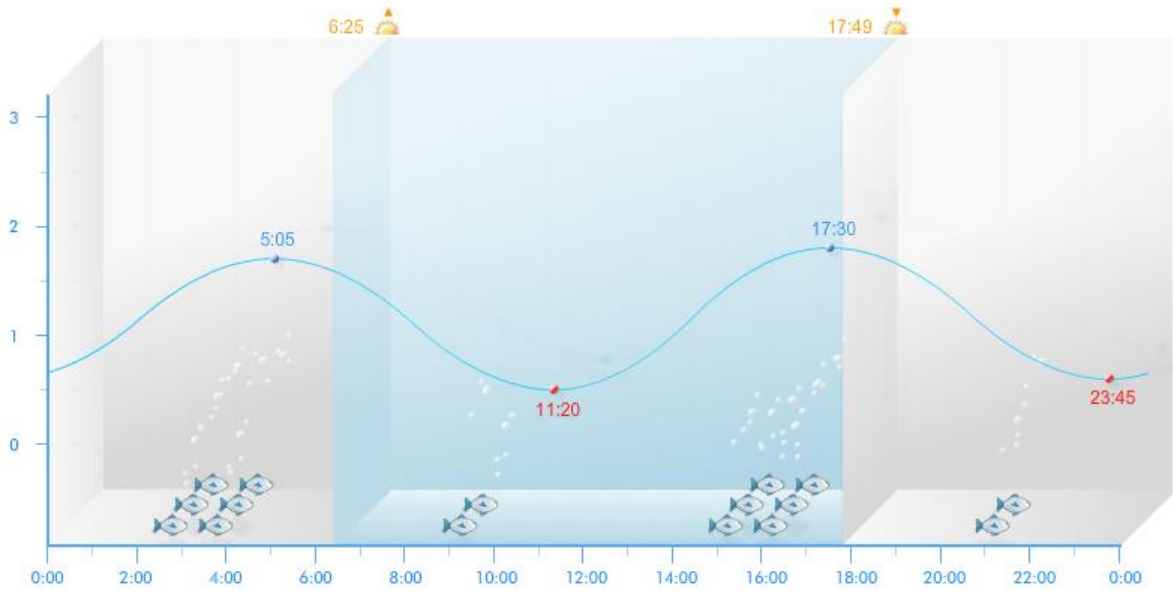

(a)

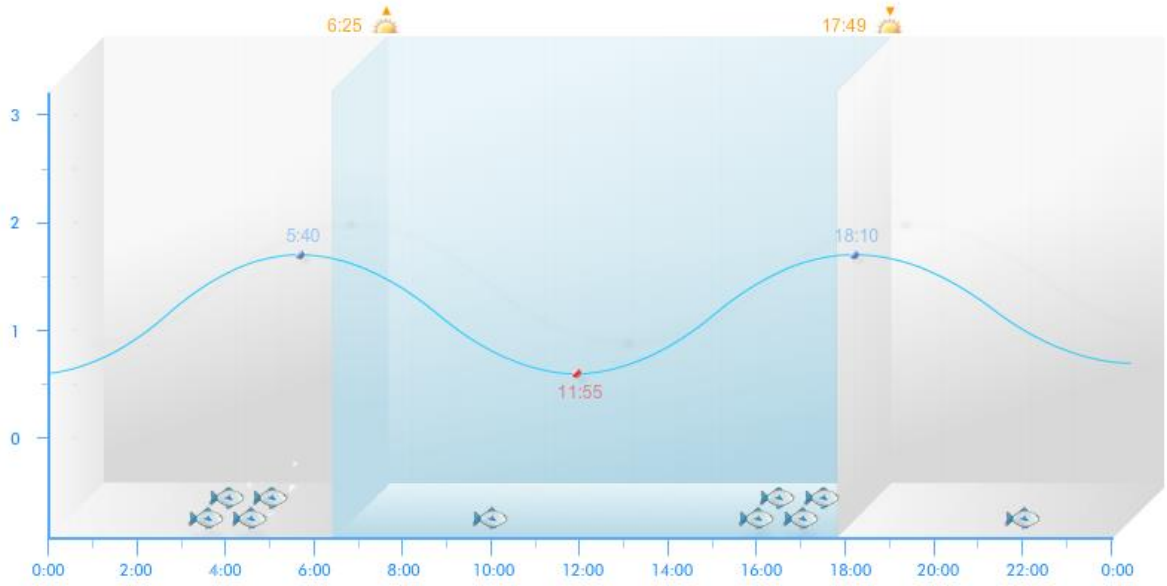

(b)

***Figure 34**- Tides plot for a) 1st day of acquisition b) 2nd day of acquisition (http://www.tabuademares.com)*